

1 **Validation of 3D-CMCC Forest Ecosystem Model (v.5.1) against**
2 **eddy covariance data for ten European forest sites**

3 A. Collalti^{1,2}, S. Marconi^{1,2}, A. Ibrom³, C. Trott², A. Anav⁴, E. D'Andrea⁵, G. Matteucci^{5,6}, L.
4 Montagnani⁷, B. Gielen⁸, I. Mammarella⁹, T. Grünwald¹⁰, A. Knohl¹¹, F. Berninger¹², Y. Zhao¹³, R.
5 Valentini^{1,2}, M. Santini¹

6 [1]{EuroMediterranean Center on Climate Change – Division on Impacts on Agriculture,
7 Forest and Ecosystem Services (IAFES), 01100 Viterbo, Italy}

8 [2]{University of Tuscia – Department for Innovation in Biological, Agro-Food and Forest
9 Systems (DIBAF), 01100 Viterbo, Italy}

10 [3]{Centre for Ecosystems and Environmental Sustainability, Dept. Chem. Engineering,
11 Technical University of Denmark (DTU), Roskilde, Denmark}

12 [4]{College of Engineering, Mathematics, and Physical Sciences, University of Exeter,
13 Exeter, United Kingdom}

14 [5]{CNR-IBAF – National Research Council of Italy, Institute of Agroenvironmental and
15 Forest Biology, 00015 Monterotondo Scalo, RM, Italy}

16 [6]{CNR-ISAQFOM – National Research Council of Italy, Institute for Agriculture and
17 Forestry Systems in the Mediterranean, 87036 Rende, CS, Italy}

18 [7]{Forest Services, Autonomous Province of Bolzano, 39100, Bolzano, Italy; and Faculty of
19 Science and Technology, Free University of Bolzano, Piazza Università 5, 39100 Bolzano,
20 Italy}

21 [8]{Research Group of Plant and Vegetation Ecology, Department of Biology, University of
22 Antwerp, Belgium}

23 [9]{University of Helsinki – Department of Physics, Division of Atmospheric Sciences,
24 00014 Helsinki, Finland}

25 [10]{Technische Universität (TU) Dresden, Institute of Hydrology and Meteorology, Chair of
26 Meteorology, D-01062 Dresden, Germany}

27 [11]{Bioclimatology, Faculty of Forest Sciences and Forest Ecology, Georg-August
28 University of Göttingen, Büsgenweg 2, 37077, Göttingen, Germany}

29 [12]{Department of Forest Sciences, University of Helsinki, POBox 27, 00014, Helsinki}
30 [13]{LOCEAN/IPSL, UMR 7159, Sorbonne Universités, Unité mixte UPMC-CNRS-IRD-
31 MNHN, 4 place Jussieu, 75005, Paris, France}
32 Correspondence to: A. Collalti (alessio.collalti@cmcc.it)

33 **Abstract**

34 This study evaluates the performances of the new version (v.5.1) of 3D-CMCC Forest
35 Ecosystem Model (FEM) in simulating gross primary productivity (GPP), against eddy
36 covariance GPP data for ten FLUXNET forest sites across Europe. A new carbon allocation
37 module, coupled with new both phenological and autotrophic respiration schemes, was
38 implemented in this new daily version. Model ability in reproducing timing and magnitude of
39 daily and monthly GPP fluctuations is validated at intra-annual and inter-annual scale,
40 including extreme anomalous seasons. With the purpose to test the 3D-CMCC FEM
41 applicability over Europe without a site-related calibration, the model has been deliberately
42 parameterized with a single set of species-specific parameterizations for each forest
43 ecosystem. The model consistently reproduces both in timing and in magnitude daily and
44 monthly GPP variability across all sites, with the exception of the two Mediterranean sites.
45 We find that 3D-CMCC FEM tends to better simulate the timing of inter-annual anomalies
46 than their magnitude within measurements' uncertainty. In six of eight sites where data are
47 available the model well reproduces the 2003 summer drought event. Finally, for three sites
48 we evaluate if a more accurate representation of forest structural characteristics (i.e. cohorts,
49 forest layers) and species composition can improve model results. In two of the three sites
50 results reveal that model slightly increases its performances although, statistically speaking,
51 not in a relevant way.

52

53 **1 Introduction**

54 Terrestrial ecosystems have a relevant role in the global carbon cycle, acting also as climate
55 regulators (Peters et al., 2007; Bonan, 2008; Huntingford et al., 2009). In fact terrestrial
56 ecosystems store large carbon stocks and cause most of the variance of carbon exchange
57 between the atmosphere and land surface (Battye Bayer et al., 2012). Among terrestrial
58 ecosystems, forests are an essential component in the global carbon cycle because of their
59 high capacity to store carbon in the vegetation and soil pools (Kramer et al., 2002). Through
60 Gross Primary Production (GPP) plants fix atmospheric carbon dioxide (CO₂) as organic
61 compounds, enabling terrestrial ecosystems to offset part of the anthropogenic CO₂ emissions
62 (Janssens et al., 2003; Cox & Jones, 2008; Battin et al., 2009). Consequently, changes in GPP
63 could have relevant impacts on atmospheric CO₂ concentration. Thus, accurately simulating
64 terrestrial GPP is key to quantify the global carbon cycle and predict the future trajectories of
65 the atmospheric CO₂ concentration (Wu et al., 2015), and taking into account the various
66 spatial and temporal scales of the processes is a major challenge (Yuan et al., 2007).
67 Terrestrial ecosystem models, used to simulate carbon, water and energy fluxes, are valuable
68 tools for advancing the knowledge of the role of ecosystems in maintaining a multitude of
69 their fundamental services, like the provision of products and the regulation of climate (Ibrom
70 et al., 2006). Such numerical models are also useful to: 1) predict the impacts of climate
71 variability on terrestrial biosphere and related carbon fluxes (Ciais et al., 2005; Brèda et al.,
72 2006; Richardson et al., 2007), ranging from long term anomalies (Santini et al., 2014) up to
73 extreme events (Zscheischler et al., 2014); and 2) reproduce biophysical and biogeochemical
74 feedbacks of vegetation cover and change on climate, especially when coupled to atmosphere-
75 ocean climate models through land surface schemes (Bonan, 2008; Arneth et al., 2012; Taylor
76 et al., 2012).

77 At European level, terrestrial ecosystems have been reported to be a significant sink of CO₂
78 (Luyssaert et al., 2012), with forests playing a relevant role in absorbing anthropogenic
79 emissions for about 10% (Nabuurs et al., 2003; UNECE and FAO, 2011).

80 In the last decade some studies have identified systematic errors when modelling terrestrial
81 ecosystem sensitivity to climate variability at multiple time scales (Friedlingstein et al., 2006;
82 Piao et al., 2013; Dalmonech et al., 2015) while sometimes differences in model predictions
83 are very large (Wang et al., 2014a).

84 To improve the models capability in reproducing relevant processes related to the land carbon
85 cycle, detailed representation of missing processes should be increasingly developed (Sykes et
86 al., 2001; Campioli et al., 2013; Nolè et al., 2013; Ciais et al., 2013; Prentice et al., 2014). For
87 instance, spatial and temporal environmental heterogeneity is known to play an important
88 role in the dynamics of populations and communities (Kobe, 1996; Chesson, 2000; Clark et
89 al., 2010; 2011). However, the implications of this heterogeneity for developing and testing
90 regional to global scale forest dynamics models that are also able to take into account forest
91 management have still largely to be explored (Zhang et al., 2014). As reported by Wramneby
92 et al. (2008), incorporating increased mechanistic details is expected to improve the
93 explanatory power of a model. Many models for example calculate leaf photosynthesis
94 through the Farquhar model (Farquhar et al., 1980; Farquhar & Sharkey, 1982), while few
95 models take in proper consideration the canopy vertical stratification. Increasing model
96 complexity can sometimes mask a lack of understanding, although models including a larger
97 subset of important processes should be more realistic than a simpler model. However,
98 complex models are tuned to perform well at standard tests but produce widely divergent
99 results when projected beyond the domain of calibration (Prentice et al., 2014). Since
100 European forests are mostly managed and not homogeneous in terms of structure,
101 composition and cohorts, only a few models are able to represent this particular ecosystem
102 complexity and heterogeneity (Grote et al., 2011; Morales et al., 2005; Seidl et al., 2012; Yin
103 et al., 2014). For simulating the impact of forest management on the carbon cycle, it is
104 important to consider the vertical structure of forests and the age-related changes in structure
105 and physiology.

106 In this study we investigate the performance of the new version of the 3D-CMCC Forest
107 Ecosystem Model (3D-CMCC FEM, Collalti et al. 2014) in quantifying GPP across different
108 forest types and climate conditions in Europe. In contrast to Dynamic Global Vegetation
109 Models (DGVMs), 3D-CMCC FEM incorporates accurate process description focusing on the
110 effects of hierarchy in vertical forest structure and ages on productivity and growth at species
111 level. The model has been designed to maintain computational efficiency, as postulated for
112 the Light Use Efficiency (LUE) Models (Monteith, 1977), coupled to the accuracy of the
113 Process-Based Models (PBMs) (Makela et al., 2000). As described by Wang et al. (2014a; b),
114 a model with both high accuracy and computation efficiency is highly desirable for the
115 purpose of simulating long time series of GPP at high spatial resolution.

116 Thanks to FLUXNET, a global network of flux tower sites, half hourly net CO₂, water and
117 energy eddy covariance (EC) flux measurements (Baldocchi, 2003) are now available for a
118 wide range of forest ecosystems. The network provides a continuously increasing set of
119 annual series of half-hourly data (Balzarolo et al., 2014). These data provide valuable
120 information to investigate seasonal phasing and amplitudes of carbon fluxes (Aubinet et al.,
121 2000; Falge et al., 2002; Gielen et al., 2013; Slevin et al., 2015) and to test terrestrial models
122 at the ecosystem scale (e.g. Richardson et al., 2010; Blyth et al., 2011; Chang et al., 2013;
123 Wißkirchen et al., 2013; Bagnara et al., 2014; Balzarolo et al., 2014; Liu et al., 2014; Wang et
124 al., 2014a; Wu et al., 2015). In the present paper daily meteorological and GPP data are
125 provided by FLUXNET. GPP data are exploited as an independent dataset to compare, over
126 different time-scales, 3D-CMCC FEM simulations for ten European forest stands varying in
127 species composition, forest structure, cohorts and climates.

128 The objective of this work is to answer the following questions:

- 129 1 Does the model reproduce the magnitude and the timing of seasonal fluctuations in GPP
130 and their effects across different forest types and forest canopy structures?
- 131 2 Does the model reproduce the observed inter-annual GPP variability?
- 132 3 Is the model generic enough so that a single set of species-specific parameterizations (i.e.
133 without a site-related calibration) allows reproducing GPP behaviour across different
134 biomes?
- 135 4 Do the model outputs improve when considering a complex heterogeneous three-
136 dimensional canopy structure compared to a simple “big leaf” model canopy
137 representation?

138 To investigate these issues, we introduced a 3D canopy representation into the 3D-CMCC
139 FEM, while however maintaining its flexibility and the generic features to be applied to
140 different forest ecosystems. The new model can now run on a daily time step and includes as
141 main changes an improved allocation-phenology scheme (with new carbon pools including
142 the non-structural carbon pool, NSC), an implemented water cycle (including snow processes)
143 and the computation of autotrophic respiration.

144

145 **2 Materials and Methods**

146 **2.1 Model description**

147 The three-dimensional Forest Ecosystem Model, 3D-CMCC FEM (Collalti, 2011; Collalti et
148 al., 2014) (source code and executables are available upon request to the corresponding
149 authors and downloadable at <http://dev.cmcc.it/git/3D-CMCC-FEM-git>) is hybrid between an
150 empirical and a process-based model relying on the concepts of the LUE approach at canopy
151 level for carbon fixation. The 3D-CMCC FEM is designed to simulate forest ecosystems at
152 flexible scale (from hectare to 1km per 1km) and on a daily time step. The model simulates
153 tree growth as well as carbon and water fluxes, at species level, representing ecophysiological
154 processes in heterogeneous forest ecosystems including complex canopy structures. The 3D-
155 CMCC FEM v.5.1 uses daily meteorological data, site-specific data and ecophysiological data
156 (e.g. maximum canopy conductance, specific leaf area, etc.; see Table S3 and Collalti et al.,
157 2014) to simulate forest processes. The model code architecture allows aggregating trees into
158 representative classes, each characterized with its variables (e.g. carbon pools, leaf area index,
159 tree height) based on their ages, species-specific and structural traits. These variables are
160 identified by the model through four indexes: i.e. species (x index), diameter class (Diameter
161 at Breast Height, DBH) (y index), height class (z index), and age cohort (k index); such
162 indexes represent the main state variables considered by the model in distinguishing
163 ecosystems across sites. To deal with forest heterogeneity within and across different
164 ecosystems, 3D-CMCC FEM v.x.x (all model versions follow the same architecture) uses a
165 species-specific parameterization for each species simulated. Moreover, based on the
166 assumption made by Magnani et al. (2007) that the above-ground net primary production
167 decreases with the ageing of a forest, the model explicitly takes into account all ages within
168 the stand, reproducing a year by year reduction due to senescence (Landsberg & Waring,
169 1997; Waring & McDowell, 2002). Height classes and the tree position within the forest
170 vertical profile are explicitly treated by the model to estimate the light availability (version
171 5.1 includes also the albedo effects) using the Monsi-Saeki formulation of exponential
172 attenuation coupled with the “Big-leaf” approach developed for a multi-layered model
173 without considering canopy depth (Collalti et al., 2014; Medlyn et al., 2003). DBH together
174 with stand density control grid cell horizontal canopy coverage (and gaps) through the
175 computation of the single tree crown coverage and then upscale to grid-cell level (Collalti et

176 al., 2014). In this way, the model is able to reproduce different combinations of uneven-aged,
177 multi-layered and multi-species forests, by optional simulation of e.g. light competition, age
178 related decline and different species-specific traits. This aspect makes the model flexible to be
179 theoretically used for a wide range of applications in forests and allows quantifying the effects
180 of a particular simulation of forest structure on model performance.

181 2.2 Model implementations

182 In this study, the 3D-CMCC FEM described in Collalti et al. (2014) has been advanced to
183 version 5.1 to improve the representation of forest processes, like phenology, canopy
184 photosynthesis, including autotrophic respiration, tree carbon allocation and water dynamics.
185 The improved phenology routine is based on a new C allocation scheme, that includes new
186 carbon pools among which the Non-Structural-Carbon (NSC) pool, related to five
187 phenological transitions for deciduous species, and three phenological transitions for
188 evergreen species, both updated once per day. Autotrophic respiration is explicitly simulated
189 and separated into maintenance and growth respiration. Maintenance respiration is the
190 function of the nitrogen content (a new added pool) in the living pools, while growth
191 respiration is computed proportionally to the carbon allocated to the different tree
192 compartments.

193

194 Photosynthesis and net primary production

195 As in the Collalti et al. (2014) the carbon flux is still estimated in 3D-CMCC FEM through
196 the Light Use Efficiency approach multiplying, for a particular species x , the absorbed
197 photosynthetic active radiation (APAR, i.e. the radiation intercepted by the canopy) with the
198 leaf area index (LAI, m^2m^{-2}) with either the prognostic potential radiation use efficiency (ε_x ,
199 grams of dry matter MJ^{-1}) or the maximum canopy quantum use efficiency (α_x , $\mu\text{mol CO}_2$
200 μmol^{-1} PAR) (for a full list of model parameters see Table S3). Parameters ε_x or α_x are
201 controlled by the product of several environmental factors (modifiers) indicated as $mod_{x,k}$
202 (dimensionless values varying between 0 and 1 and differing for each species x and age class
203 k) depending on: vapour pressure deficit, daily maximum and minimum air temperatures, soil
204 water content and site nutrient status (for a full modifiers description see Landsberg &
205 Waring, 1997). Gross Primary Production (GPP; $\text{gCm}^{-2}\text{day}^{-1}$) is thus calculated using the
206 following equation:

207 $GPP_{x,y,z,k} = (\varepsilon_x \text{ or } \alpha_x) * APAR_z * mod_{x,k}$ (1)

208 where $APAR_z$ is the absorbed radiation by the trees at the z^{th} layer (where z represents the
209 layer of representative height for each height class).

210 Conversely from the previous version where Autotrophic Respiration (AR) was set as a
211 constant fraction of GPP (Waring & Landsberg, 1998), in this version AR is explicitly
212 simulated. AR is treated distinguishing into Maintenance Respiration (MR), governed by a
213 Q_{10} type response function (Ryan, 1991; Bond-Lamberty et al., 2005) and Growth Respiration
214 (GR) assumed to be a constant proportion (30%) of all new tissues produced (Larcher, 2003).
215 Net Primary Production (NPP), is then calculated as follows:

216 $NPP_{x,y,z,k} = GPP_{x,y,z,k} - AR_{x,y,z,k}$ (2)

217 NPP is then partitioned into biomass compartments and litter production following dynamic
218 allocation patterns that reflect environmental constraints (i.e. light and water competition) and
219 age.

220

221 Daily meteorological forcing and snow dynamics

222 The model implements a daily time step (previous version was at monthly time step) thanks to
223 the temporal frequency of meteorological forcing input data: daily maximum (T_{max} ; °C) and
224 minimum air temperature (T_{min} ; °C), soil temperature (T_{soil} ; °C), vapour pressure deficit (hPa),
225 global solar radiation ($MJ\ m^{-2}\ day^{-1}$) and precipitation amount ($mm\ day^{-1}$). In addition, the
226 model uses the day-time (T_{day} ; °C) and night-time (T_{night} ; °C) average temperature computed
227 as follows (Running & Coughlan, 1988):

228 $T_{day} = 0.45 * (T_{max} - T_{avg}) + T_{avg}$ (3)

229 $T_{night} = (T_{day} + T_{min})/2$ (4)

230 Where T_{avg} is the daily average air temperature (°C). When the soil temperature is missing
231 among in situ observed data, the model estimates it for the upper 10 cm of the soil layer
232 through an 11-day running weighted average of T_{avg} and further corrected by the presence of a
233 snowpack as in Thornton (2010), Kimball et al. (1997) and Zeng et al. (1993). The variable
234 related to the snowpack thickness was included as a water cycle component by reproducing
235 the daily amount ($mm\ day^{-1}$) of snow melt driven by average air temperature (T_{avg}) and
236 incident net global radiation (Rad_{soil} ; $W\ m^{-2}$), while snow sublimation is only driven by T_{avg} .

237 In case of snow presence, if T_{avg} is higher than 0°C, considered the melting point as in
238 Running & Coughlan (1988) and Marks et al. (1992), the rate of daily snowmelt is estimated
239 by:

240
$$Snow_{melt} = (t_{coeff} * T_{avg}) + \left(\frac{Rad_{soil} * \varepsilon_{snow}}{H_{fus}} \right) \quad (5)$$

241 where t_{coeff} is the snowmelt coefficient ($0.65 \text{ Kg m}^{-2} \text{ }^{\circ}\text{C}^{-1} \text{ day}^{-1}$), ε_{snow} is the absorptivity of
242 snow (0.6), H_{fus} is the latent heat of fusion (335 kJ kg^{-1}), Rad_{soil} is the incident net global
243 radiation at the soil surface ($\text{kJ m}^{-2} \text{ day}^{-1}$).

244 Otherwise, if T_{avg} is lower than 0°C snow sublimation is computed by:

245
$$Snow_{subl} = \left(\frac{Rad_{soil} * \varepsilon_{snow}}{H_{sub}} \right) \quad (6)$$

246 where H_{sub} is the latent heat of sublimation (2845 kJ kg^{-1}).

247

248 **Phenology and Carbon allocation**

249 Phenology plays a fundamental role in regulating photosynthesis and other ecosystem
250 processes (e.g. carbon and nitrogen dynamics), as well as inter-individual and inter-species
251 competitive relations and feedbacks to the climate system (Richardson et al., 2012a). In the
252 updated model version phenology and carbon allocation depend on six different carbon and
253 nitrogen pools (while three carbon pools where considered in the previous versions). Five
254 pools represent the main tree organs: foliage, (fine and coarse) roots, stem, branch and bark
255 fraction. One new pool corresponds to non-structural carbon (NSC; starch and sugar) stored in
256 the whole tree. The inclusion of this new pool was necessary to represent NSC mobilization
257 and consequently leaf phenology (e.g. leaf production during spring for deciduous trees) and
258 carbon allocation. Woody pools are furthermore distinguished between live and dead wood.
259 In the new version of 3D-CMCC FEM, LAI values are predicted for sun and shaded leaves
260 (De Pury & Farquhar, 1997; Thornton & Zimmermann, 2007; Wu et al., 2015), minimizing
261 the effects of the “Big-leaf” approach (Monteith, 1965; Sellers et al., 1997), as a function of
262 the amount of carbon allocated to the leaf pool. It is noteworthy that each pool and each
263 structural state variables is daily updated according to the meteorological data, forest structure
264 and simulated fluxes.

265 Following Arora & Boer (2005), for deciduous species the model considers five phenological
266 transitions (being just four in the previous versions: bud burst, peak LAI, leaf fall period and
267 dormancy) that drive the seasonal progression of vegetation through phases of
268 dormancy/quiescence, budburst, maximum growth, active growth, and senescence as in the
269 following:

- 270 1. Leaf onset starts from quiescence when thermic sum (the sum of the T_{day} air
271 temperatures exceeding the threshold T_{base} value of 5°C) exceeds a species- and site-
272 specific temperature threshold value (Rötzer et al., 2004; Dufrene et al., 2005) and
273 when the LAI value reaches $LAI = \max(LAI) * 0.5$. The costs of expanding buds
274 during this period of high carbon demand are supported by NSC (Landhausser, 2010;
275 Dickmann & Kozlowski, 1970).
- 276 2. During the budburst phase, carbon and NSC are allocated to the foliage pool, as long
277 as the balance between GPP and AR is positive (Barbaroux & Bréda, 2002; Campioli
278 et al., 2013; Scartazza et al., 2013).
- 279 3. During the succeeding maximum growth phase and lasting up to peak LAI, carbon is
280 allocated into foliage and fine root pools (Sabatè et al., 2002), based on the pipe model
281 theory (Shinozaki et al., 1964 a; b), to optimize photosynthesis; otherwise, no growth
282 occurs and NSC is used.
- 283 4. Successively, the full growing phase lasts up to the day when day length (in hours) is
284 shorter than a species-specific threshold value. In this phase carbon is allocated into
285 stem, fine and coarse roots, branch and bark, and into non-structural carbon pools in
286 order to refill the reserves for the next years.
- 287 5. Finally, during the leaf fall (i.e. yellowing or senescence) phase, lasting until the leaf
288 fall (assumed linear) is complete, the total positive carbon balance is allocated to the
289 NSC pool.

290 Outside the growing season (dormancy) trees consume NSC for fuelling maintenance
291 respiration (Ogren, 2000).

292 For evergreen species the model follows a similar but simplified approach simulating a first
293 maximum growth phase, when the model allocates NSC to foliage and fine roots up to reach
294 peak LAI, and a second full growing phase, when the model allocates to the other pools. As in

295 Lawrence et al. (2011) for litterfall we assume and simplify that there are no distinct periods,
296 but rather a continuous shedding of foliage and fine roots of the previous years.

297 All tree pools are updated at a daily time step depending on NPP balance. Nitrogen
298 concentration for each pool is considered as a C/N ratio following Dufrene et al. (2005) and
299 Thornton (2010). The C/N stoichiometry is constant and depends on species; unfortunately,
300 the model still lacks of an interactive C-N cycle. Forest stand structural attributes, e.g. DBH,
301 tree height, and crown competition are also updated at a daily time step based on species-
302 specific biometric relationships.

303

304 **Autotrophic respiration**

305 Based on the approach of BIOME-BGC model (Thornton, 2010) 3D-CMCC FEM computes
306 the daily AR of all living tissues. MR is a modified Van't Hoff function (Davidson et al.,
307 2006; Mahecha et al., 2010) of temperature with the temperature sensitivity parameter Q_{10}
308 (see below) and a linear function of the nitrogen content ($N_{content} = 0.218 \text{ kgC kgN}^{-1} \text{ day}^{-1}$;
309 Ryan, 1991) in the living compartments. The Q_{10} function is an exponential function for
310 which a 10°C increase in temperature relates to a Q_{10} factor change in the rate of respiration.
311 MR is partitioned into day time and night time respiration using, in place of *temp* in Eq.(7):
312 t_{day} and t_{night} for foliage, t_{soil} for fine and live coarse roots, and t_{avg} for live stem and branch.

313
$$MR_{x,y,z,k} = 0.218 * N_{content}_{x,y,z,k} * Q_{10}^{(temp-20)/10} \quad (7)$$

314 $GR_{x,y,z,k}$ is considered as a fixed ratio (30%) of all newly grown (i.e. living) tissues as
315 proposed by Larcher (2003).

316

317 **2.3 Data description**

318 Model validation has been performed for ten different forest sites (Table 1) included in the
319 European EC fluxes database cluster (URL: <http://www.europe-fluxdata.eu>). For each site,
320 3D-CMCC FEM v.5.1 simulations were performed averagely for 10 years, forced with gap-
321 filled daily meteorological data, according to the available time series. The selected sites
322 cover a wide range of European forest ecosystems across different latitudes, landscapes and
323 three climatic zones: temperate, Mediterranean and subalpine.

324 For all sites, daily time series of meteorological variables (maximum and minimum air
325 temperature, precipitation, vapour pressure deficit and incoming solar global radiation) were
326 used as drivers, while GPP was used for model output validation. The GPP derives from Net
327 Ecosystem Exchange (NEE) measurements that have been previously quality checked and
328 processed including storage correction, spike detection, and low turbulence condition (u^*)
329 filtering according to the method in Papale et al. (2006) and gap filled using the Marginal
330 Distribution Sampling method (MDS; Reichstein et al., 2005). The GPP is not directly
331 measured by the eddy covariance technique but it is estimated using a partitioning technique
332 as described in Reichstein et al. (2005). In the rest of the paper, we will refer to these data as
333 “measured” or “observed” GPP for simplicity but it is important to highlight that they are
334 obtained using a modeling approach (although strongly based on direct measurements).

335 2.4 Model and experimental set-up

336 Site data needed for model initialization concerned information on forest structure (DBH, tree
337 height, age and density), its species composition, and soil characteristics (e.g. soil depth,
338 texture and bulk density). These data were used for each site to initialize the model, i.e. to
339 describe soil characteristics and the initial forest conditions at which the model starts to
340 simulate forest processes. Initialization data were taken from the BADM (Biological,
341 Ancillary, Disturbance, Metadata) files, available at <http://www.europe-fluxdata.eu>, for each
342 of the selected sites, and complemented by a literature review and personal contacts with the
343 sites’ Principal Investigators. Length of model simulations, basic sites description and forest
344 attributes used for model initialization are shown in Table 1. As a whole, for all sites, the
345 species-specific ecophysiology has been parameterized generically (i.e. not related to the
346 simulated site) using only data from the literature (e.g. Breuer et al., 2003; Mollicone et al.,
347 2003; Pietsch et al., 2005; White et al., 2000) independently from site-related measurements
348 (for a list of model ecophysiological and structural species-related parameters see Table S3).
349 As in White et al. (2000) and in Naudts et al. (2014) in case of multiple values available for a
350 single parameter, the mean values were used. Using the mean parameter estimates avoided
351 hidden model-tuning (i.e. the use of unrealistic value to obtain the best fit) and largely reduces
352 the likelihood that simulation results are biased by hidden calibration.

353 In addition, several studies (Bolstad et al., 1999; Griffin et al., 2001; Ibrom et al., 2006;
354 Misson et al., 2007; Cescatti et al., 2012; Guidolotti et al., 2013; Migliavacca et al., 2015)

355 claim that beside environmental variables, spatial heterogeneity (horizontal and vertical) of
356 the stand structure and composition (age, species) also plays an important role at the
357 ecosystem level. To evaluate if a more detailed simulation of forest heterogeneity improves
358 model performances, a number of replicated simulations were performed for three
359 heterogeneous sites (BE-Bra, IT-Ren and DE-Tha), based on different model initializations in
360 terms of forest layers, species composition and/or ages (Table 1). These replicates start from a
361 forest representation very close to reality (e.g. cohorts, mixed species composition and
362 different canopy layers) to a more generalized one. For reasons of comparability, in these test
363 sites the model has been forced with the same meteorological input data, and eco-
364 physiological species-related parameterizations, i.e. only model initializations data, related to
365 stand attributes, differ. These data are based on different sources: site measurements and/or
366 literature data and/or experimental settings.

367 In the case of BE-Bra we initialized the model with near all possible combinations of
368 initialization datasets. The first simulation (BE-Bra P_Q-3L) has explicitly taken into account
369 the site heterogeneity (vertical and horizontal) (following Gielen et al., 2013, and ancillary
370 data sources) consisting in mixed species composition at a different canopy coverage rate of
371 *Quercus robur* (Q) and *Pinus sylvestris* (P) (20 and 80%, respectively), with two cohorts
372 (oaks and pines, 65 and 72 years old, respectively) and three forest layers. In the second
373 simulation (BE-Bra P), only a single-layer of Scots pines was considered (following Janssens
374 et al., 2002 and Verbeeck et al., 2007). In the third, fourth and fifth simulations (BE-Bra
375 Q_3L, BE-Bra Q_2L, BE-Bra Q_1L, respectively) only three, two and one layer of
376 pedunculate oaks (following Curiel Yuste et al., 2005 and experimental set up) were assumed.
377 Additionally, two more experimental set-ups combined two layers of oak and one layer of
378 pine (BE-Bra P_Q-2L) and one layer of oak and pine (BE-Bra P_Q-1L).

379 For IT-Ren, in the first simulation, two layers and two cohorts were considered (IT-Ren
380 2L_2C) following Montagnani et al. (2009). In the second case, stand heterogeneity has been
381 grouped into one layer, i.e. minimizing forest structure, and one single averaged cohort (IT-
382 Ren 1L_1C; experimental set up).

383 For DE-Tha, two species (DE-Tha 2S) (spruce 80% and pine 20%, respectively) were
384 modelled in the first simulation (following Grünwald & Bernhofer, 2007), while in the second
385 experiment only the dominant species (spruce; DE-Tha 1S) was considered (BADM source).

386 2.5 Validation approach

387 In order to analyse model performance, we used daily (X_{daily}), monthly (X_{monthly}) and annual
 388 (X_{annual}) time series for modelled and observed GPP values, which were compared at the
 389 different time scales. At first, we conducted a comparison via appropriate performance indices
 390 on long-term annual average (i.e. over the full series of all the available years), then we
 391 evaluated how the model performed in the different seasons aggregating values for months of
 392 the same season.

393 In addition, to avoid misleading results in the daily and monthly signal comparisons due to the
 394 strong seasonality for both daily and monthly signals, we followed the decomposition
 395 technique proposed by Zhao et al. (2012). To partially remove the seasonal cycle signal, we
 396 build a new daily (Y_{daily}) and a new monthly (Y_{monthly}) dataset for both observed and modelled
 397 data, respectively. The Y_{daily} is created by subtracting the daily time series from the daily
 398 mean of the month, and the Y_{monthly} by subtracting the monthly time series from the annual
 399 mean (see Table S1-b).

400 For both X and Y datasets we firstly adopted the Pearson coefficient of correlation (r). Then,
 401 we calculated the Normalized Root Mean Square Error (NRMSE) (Anav et al., 2010; Keenan
 402 et al., 2012) as a standardized index of error. The NRMSE reports the mean difference
 403 between observed and modelled GPP values (GPP_{EC} and GPP_{MD} , respectively) normalized on
 404 the variability in the GPP_{EC} , in order to have an indication of the average distance between
 405 GPP_{MD} and GPP_{EC} , comparable among the different sites. NRMSE was quantified as:

$$406 NRMSE_{GPP} = \frac{\sqrt{\sum_{i=1}^N (GPP_{ECi} - GPP_{MDi})^2}}{\sum_{i=1}^N \sigma(GPP_{ECi})} \quad (8)$$

407 where i represents the day (or month), and $\sigma(GPP_{EC})$ is the standard deviation of the full daily
 408 (or monthly) series of observed GPP consisting of N records.

409 In addition, model performances were measured for the same series through the ‘Model
 410 Efficiency’ index (MEF) following Reichstein et al. (2002) and Migliavacca et al. (2015):

$$411 MEF = 1 - \frac{\sum_{i=1}^N (GPP_{ECi} - GPP_{MDi})^2}{\sum_{i=1}^N (GPP_{ECi} - \text{avg}(GPP)_{EC})^2} \quad (9)$$

412 In contrast to correlation coefficient r , the MEF index (Bowman & Azzalini, 1997) measures
 413 not only the correlation between modelled and observed data (in other words, how well they

414 reproduce the phase of observations), but also their ‘coincidence’, i.e. the deviation from the
415 1:1 line, and it is sensitive to systematic deviations between model and observations
416 (Reichstein et al. 2002).

417 Another index used in model evaluation is the standardized Mean Absolute Bias (MABstd)
418 (Li et al., 2010) instead of classical Bias index to avoid compensations for errors of opposite
419 signs and standardized (as for NRMSE) to allow comparison across sites:

$$420 MABstd = \sum_{i=1}^N \left(\frac{|GPP_{MD_i} - GPP_{EC_i}|}{\sigma(GPP_{EC_i})} \right) \frac{1}{N} \quad (10)$$

421 To evaluate the model performances in terms of variability patterns, we adopted a procedure
422 to compare each GPP_{MD} value to both its correspondent GPP_{EC} value and the GPP_{EC} - GPP_{MD}
423 difference, at daily and monthly levels. Since the different sites have different ranges of GPP,
424 we arranged in ascending order GPP_{EC} time series, then divided the whole series in 18 classes,
425 each one containing values of a 5 percentile class. For each group of GPP_{EC} we calculated the
426 median and reported the range. We calculated the same statistics for the values of GPP_{MD}
427 arranged so that dates of GPP_{MD} and GPP_{EC} matched. We chose the median rather than the
428 average because it is less influenced by outliers. We decided to use the range rather than the
429 variance as a measure of variability, because giving information on asymmetry.

430 In order to assess the Inter-Monthly and Inter-Annual Variability (IMV and IAV
431 respectively), individual GPP values for each month and year considered were normalized
432 following Vetter et al. (2008) and Keenan et al. (2012). Shortly, we subtracted the respective
433 observed or modelled average from individual (monthly and yearly) observed and modelled
434 value as follows:

$$435 IMV_{(EC \text{ or } MD)i} \text{ or } IAV_{(EC \text{ or } MD)i} = GPP_{(EC \text{ or } MD)i} - avg(GPP)_{(EC \text{ or } MD)} \quad (11)$$

436 where $avg(GPP)$ is the long-term (full series of all the available years) average of monthly
437 (for IMV) or yearly (for IAV) GPP from observations (EC) and modeling (MD), respectively.
438 A kernel density estimation (*kde*) was performed to qualitatively observe probability
439 distribution functions (PDFs) respectively of the IMV and IAV values (Bowman & Azzalini,
440 1997).

441 To evaluate 3D-CMCC FEM ability in reproducing the observed IMV and IAV, we
442 calculated the NRMSE based on monthly and annual time series of IMV and IAV values,
443 respectively. The NRMSE, adopted as a normalized index of error allowing comparability

444 among different sites, was thus calculated as in Eq. 8 but using IMV and IAV instead of GPP
445 individual values, following the approach of Keenan et al. (2012).

446 **3 Results**

447 **3.1 GPP evaluation over long-term annual and seasonal scale**

448 Both monthly and daily simulated (MD) GPP show high correlations with EC data and these
449 results are consistent with MEF values as well as with NRMSE and MABstd (Table S1a, and
450 Figure 1-a and 1-b). On average, deciduous forests reveal better correlation between MD and
451 EC data than evergreen forests, with a mean r of 0.86, while evergreen and mixed stands
452 show average r of 0.81 and 0.77, respectively. For all stations $p < 0.0001$. These results are
453 confirmed by Taylor diagrams (Taylor, 2001) (Figure 2a) which show that the model
454 performs satisfactorily for daily fluxes, in four (i.e. DE-Hai, DK-Sor, DE-Tha, FI-Hyy) of ten
455 sites falling within ± 0.5 normalized standard deviations from the reference point (REF;
456 representing observed data) and having correlation around 0.9. For six sites (all the evergreen
457 needleleaf plus deciduous except FR-Hes), the normalized standard deviation of simulated
458 data is close to that of observed data (represented by reference line with normalized standard
459 deviation, i.e. radial distance from the axis origin equal to 1). Simulated data for IT-Cpz, FR-
460 Hes and FR-Pue have, respectively, a normalized standard deviation of approximately +0.2,
461 +0.3 and +0.4 (as difference from that of observations) consistently with the lower correlation
462 values; BE-Bra shows the highest negative difference, in terms of standard deviation, of
463 around -0.3. On average, the least performing result is for IT-Cpz that shows a correlation
464 below 0.60 and falls outside ± 1 normalized standard deviation from the reference point. The
465 Taylor diagram in Figure 2b shows the model's capability to better simulate GPP at monthly
466 scale. For seven sites (all deciduous and evergreen needleleaf), the normalized standard
467 deviations of modelled data are close to that of observations (reference line), the correlation is
468 well above 0.90 and within ± 0.5 normalized standard deviation from the reference point. IT-
469 Cpz and BE-Bra show improved results with respect to daily data: respectively, their
470 correlation increases by more than 0.1 units, they fall within the +0.2 and -0.2 units of
471 normalized standard deviation differences with respect to that of observations, and they enter
472 in the field of ± 1 and ± 0.5 normalized standard deviation from the reference point,
473 respectively, although for IT-Cpz the values for all statistical indexes are consistently the
474 lowest. Although less strongly, FR-Pue monthly data also have better performances than daily

475 data results in terms of higher correlation (0.89) and closer position in terms of normalized
476 standard deviations units from the reference point even if the other indexes are a little bit far
477 from the average values of the other sites.

478 To reduce the effects of seasonality, we also examine model performance using
479 decomposition method (section 2.5). In the daily time-step, the overall model performance is
480 much lower in Y dataset (Figure 1-c and Table S1b) than in X dataset, that is, $r= 0.51$, $MEF =$
481 -0.43 , $NRMSE = 1.18$ and $MABstd = 0.8$ in Y dataset vs $r= 0.82$, $MEF = 0.63$, $NRMSE =$
482 0.57 and $MABstd = 0.44$ in X dataset. The large model error at synoptic scale have been well
483 recognized by previous studies (Dietze et al., 2011; Zhao et al., 2012). The model shows to be
484 a good predictor for DE-Tha and FR-Pue and to be less predictive for DK-Sor and FR-Hes
485 with respect to the X dataset. Accordingly, for FR-Pue comparisons between X and Y datasets
486 show that this site is less affected by seasonality while DK-Sor is the most affected one. As
487 expected, in the monthly time step, the decomposition technique returns more similar results
488 between X and Y datasets. Worst results are for IT-Cpz while best results are for DE-Hai,
489 DK-Sor, DE-Tha and IT-Ren (see Table S1b and Figure 1-d). Overall, after smoothing the
490 seasonality the model shows to be slightly better predictive with average values among sites
491 consistent with observed data ($r = 0.94$, $MEF = 0.85$, $NRMSE = 0.36$ and $MABstd = 0.27$).
492 Comparison between X and Y datasets shows that DE-Hai is less affected by seasonality and
493 IT-Cpz is the most affected one. In brief, comparison between X and Y datasets shows similar
494 reconstruction ability in the monthly time step, but very different in the daily time step
495 because X dataset contains the feature of large seasonality. Given that one of the objects of
496 this study focuses on seasonality fluctuation, we mainly show the results based on X dataset
497 hereafter without specification.

498 To summarize, although with similar inter-sites variability, monthly correlations across
499 different sites are higher than daily ones, with average correlations of 0.94 for deciduous, 0.90
500 for evergreen and 0.92 for mixed stand (Figure 1 and Table S1a).

501 Daily and monthly NRMSE are usually less than 1.00. Monthly NRMSE is less than daily
502 NRMSE, 0.41 vs. 0.63 on average, respectively (Table S1a). These results confirm that the
503 model performs better at a monthly than at a daily time scale (Figure 1), likely because of
504 averaging effects of daily variability in GPP estimation.

505 The same consistency is shown for MEF index that is on average 0.79 (monthly) and 0.57
506 (daily), with largely lower values for the two Mediterranean forests (IT-Cpz and FR-Pue) at
507 both the daily and monthly time scale (Table S1a and Figure 1).

508 Considering the annual mean in deciduous forests (Table S1a), the model slightly
509 underestimates the GPP by -2.4% (average among DE-Hai, DK-Sor), while in FR-Hes and
510 IT-Col it shows an overestimation of 5.2% on average. Concerning evergreen forests, we find
511 an overall model underestimation of 2.1%, with higher variability compared to deciduous
512 forests, and more divergent in the case of the two Mediterranean ecosystems, ranging from
513 underestimation of 18.4% ($318 \text{ gC m}^{-2} \text{ year}^{-1}$; IT-Cpz) to overestimation of 12.1% ($158 \text{ gC m}^{-2} \text{ year}^{-1}$; FR-Pue). Results for the mixed forest site of BE-Bra are reasonable, with an
515 underestimation of about 4.4%.

516 In terms of inter-annual variability of the yearly mean, GPP_{MD} falls well within the range of
517 GPP_{EC} standard deviations for all sites except at IT-Cpz (Figure 3). Deciduous broadleaved
518 and the evergreen needleleaf are the best reproduced.

519 Performance indices from daily and monthly observed and modelled GPP series analysed at
520 seasonal level are shown in Table S2 and Figures 4 and 5. Winter (DJF) and summer (JJA)
521 correlations were generally lower than those in autumn (SON) and spring (MAM).
522 Specifically, DJF and JJA showed a correlation of 0.45 and 0.46 respectively on a daily scale
523 and a value of 0.59 and 0.50 on a monthly scale; MAM and SON showed on a daily scale an
524 average correlation of 0.72 and 0.77 respectively, while on monthly scale a correlation of 0.82
525 and 0.86 with two low values of 0.05 and 0.06 for monthly DJF and MAM for IT-Cpz was
526 shown. Winter and summer monthly average NRMSE of 1.13 and 1.00, respectively, were not
527 significantly different to the 0.66 and 0.57 of spring and fall. MEF and MABstd indexes
528 values suggest similar findings than NRMSE.

529 Figure 6 shows overall modelled vs. observed fluxes over daily and monthly scales, and the
530 absolute difference ($\Delta \text{GPP}_{\text{MD}}$, i.e. GPP_{MD} minus GPP_{EC}) vs. observed fluxes (GPP_{EC}) as
531 calculated by the difference matrix described in section 2.5. Overall, the aggregated data
532 reveal high correlation also due to a progressively reduced range of data, and then variability,
533 at higher GPP values (Figures 6; top plots). Figures 6 (bottom plots) show patterns of $\Delta \text{GPP}_{\text{MD}}$ with
534 increasing GPP_{EC} . These differences result in strong reduction of discrepancies for
535 GPP_{EC} greater than $8.5 \text{ gC m}^{-2} \text{ d}^{-1}$ for daily, or $7.3 \text{ gC m}^{-2} \text{ d}^{-1}$ for monthly time series.

536 The average intra-annual GPP variations are analysed by calculating the long-term average
537 and standard deviation values for each month of the year (Figure 7). In spring, the modelling
538 results from deciduous forests present a larger variability than the observed data, especially
539 during budburst and in late spring. The model generally matches the observed phenology
540 timing (budburst, peak LAI, leaf senescence and their fall, i.e. length of growing season, data
541 not shown). Consistent biases were observed in late summer.

542 3.2 Inter-monthly and inter-annual variability

543 The distribution of the IMV for the analysed sites reveals in general lower variance for
544 modelled than observed data (Figure 8 and Table 2). Regarding deciduous forests, both DK-
545 Sor and FR-Hes show IMV_{MD} distributions with a larger interquartile range in comparison
546 with IMV_{EC} (p -value < 0.05). Conversely, for DE-Hai and IT-Col the IMV_{MD} variance is
547 statistically representative for the IMV_{EC} ; however IT-Col shows a significantly biased
548 median (p -value < 0.05). Less variability than IMV_{EC} is generally observed for IMV_{MD} of
549 conifers. While DE-Tha shows significant agreement for both variance and central tendency
550 (median) (p -value > 0.05), at FI-Hyy the IMV_{MD} appears statistically in disagreement with
551 IMV_{EC} for both variance and central mean tendency (p -value < 0.05). We find a small
552 difference between IMV_{MD} and IMV_{EC} probability density modal values in IT-Ren (Table 2).
553 Concerning broadleaved evergreen vegetation, we observe very good agreement between
554 observed and modelled IMV central tendency measures in FR-Pue with most of the
555 frequencies between $\pm 2 \text{ gCm}^{-2}\text{d}^{-1}$. In FR-Pue, however, we notice that the distributions are
556 slightly shifted, especially around the median, with resulted variance from modelled data in
557 disagreement with observed data. We detect high IMV distributions disagreement in IT-Cpz,
558 where the PDF from observed IMV is normally distributed and the one from modelled IMV is
559 not (as resulted by a χ^2 goodness of fit test). IMV_{MD} series in BE-Bra (mixed forest) are in
560 low agreement with those from EC. Modelled variance is low, and positive IMV values are
561 especially scarcely represented. Table 2 also shows the NRMSE for IAV and IMV series.
562 There is no apparent correlation either between sites species and average error, or between
563 distributions uniformity and NRMSE. In fact, the lowest NRMSE for IMV was found in BE-
564 Bra and IT-Col and the highest in DE-Hai and DK-Sor. On average the model has a NRMSE
565 for IMVs of about 1.2.

566 Figure 9 shows the modelled and measured individual IAV values for each studied site. The
567 magnitude of IAV_{MD} was on average of the same order as IAV_{EC} , showing the model's ability
568 to reproduce the inter-annual variability range, and capturing about 62% of the anomalies
569 signs (i.e. timing) for the total set of years. The model generally better captured conifers' IAV
570 sign (i.e. DE-Tha, FI-Hyy, and IT-Ren), with 66% of the times against about 59% for the
571 deciduous forests (i.e. DE-Hai, DK-Sor, FR-Hes, IT-Col) and 55% for the Mediterranean
572 ones (i.e. FR-Pue and IT-Cpz). However, the IAV difference in magnitude was better
573 represented for deciduous forests rather than conifers, as inferred by the average NRMSE of
574 respectively 1.45 and 1.67 (calculated by averaging values reported in Table 2). Although the
575 model reproduced the timing of anomalies satisfactory in more than half of cases (a little bit
576 more than in a random selection), the correlations had a wide spread across sites.
577 Quantitatively, modelled anomalies suggest better results for FR-Pue ($r = 0.76$) and worse
578 results for IT-Ren ($r = -0.54$).

579 In the case of the year 2003 with its summer heat and drought extreme (Ciais et al., 2005;
580 Vetter et al., 2008), the anomaly sign has been well captured by the model for six of the eight
581 sites analyzed for that year (no observations were available for BE-Bra and IT-Ren) (Figure
582 9). At IT-Cpz and DK-Sor, average IAV_{MD} has the opposite sign to IAV_{EC} , while 2003 was
583 recognized as not remarkably anomalous at IT-Col. Similarly, the model results match with
584 that found by Delpierre et al. (2009) about the anomalous carbon uptake during the warm
585 spring of 2007 compared with the decadal mean for FR-Pue, FR-Hes, and DE-Tha.

586 3.3 Comparison within different forest structure simulations

587 Considering the presence of only one species (either pines or oaks) strongly limits the model
588 to simulate the daily and monthly GPP patterns in BE-Bra (Table 3). This site represents a
589 mixed stand of deciduous and evergreen tree species that assimilates CO_2 all year round,
590 although low temperatures in winter and spring reduce photosynthesis for pines also. The
591 observed GPP fluxes are then caused by the 'mixture', at a varying degree, of both oak and
592 pine trees. Considering BE-Bra as a pure oak forest with a variable number of layers
593 (simulation codes: BE-Bra Q_3L, BE-Bra Q_2L, BE-Bra Q_1L) the model results for annual
594 GPP deviate from -1.2 up to -7.4%; considering a pure pine forest (BE-Bra P) or a
595 combination of pines and one layer of oak (BE-Bra P_Q-1L) the model underestimates
596 annually from -15.9% to -11.5%, respectively. It is noteworthy that the daily GPP values

597 show a markedly different seasonal distribution on fluxes (data not shown). Conversely, there
598 is no clear evidence that in simulating pines coupled with one, two or three oak layers (BE-
599 Bra P_Q-1L, BE-Bra P_Q-3L BE-Bra P_Q-2L) model results largely benefitted of this
600 differentiation both on a daily, monthly and annual scale. Similar results are obtained for DE-
601 Tha site when simulating one single species (DE-Tha 1S) or two (DE-Tha 2S), since the
602 similar phenology behaviour of modelled species does not cause a marked difference in the
603 seasonal GPP cycle. On the other hand, IT-Ren initialized as a single layer and with one
604 single cohort (IT-Ren 1L_1C) instead of two layers and two cohorts (IT-Ren 2L_2C) differs
605 strongly from observed GPP values overestimating the annual cumulated GPP by 43.2%.
606 However, for this site, the analysis of performance indices based on daily and monthly series
607 shows no evidence of improved model results.

608 4 Discussion

609 In this paper, we have analyzed the capability of the latest version of the 3D-CMCC FEM
610 (v.5.1) to simulate intra-annual to inter-annual GPP variability over ten heterogeneous
611 European forest sites, representative of different ecosystems and bioclimatic regions, by
612 comparing model results with observations based on the EC technique. Although the model
613 provides a reasonable reproduction of the observed values, we may evince some critical
614 issues. First, the observed GPP data are affected by high uncertainties (Kenan et al., 2002;
615 Papale et al., 2006; Richardson et al., 2012a, b). According to Luyssaert et al. (2007) these
616 uncertainties in the ten case studies considered here, although at the biome level, have a very
617 high spread, varying from ± 557.9 (for FI-Hyy) to ± 700 $\text{gC m}^{-2}\text{yr}^{-1}$ (for IT-Cpz). Besides
618 uncertainty in the EC technique, model assumptions and parameterizations can increase
619 discrepancies compared to observed GPP data.

620 A potential further source of error in the model runs that may need to be considered or
621 accounted for is related to our choice of not making a site-specific parameterization. Since we
622 used general parameterizations, large uncertainties could be detected especially in the
623 variables that determine, for example, the length of the growing season (Richardson et al.,
624 2010), and the latitudinal differences (acclimation) of the maximum, minimum and optimum
625 temperatures for photosynthesis. Improvement could be achieved with a site-specific
626 parameterization, but this falls beyond our goal to make the model generally applicable. In
627 addition, to avoid a misleading model evaluation coming from strong seasonality (especially
628 for deciduous sites) we followed the decomposition technique proposed by Zhao et al. (2012).

629 On average, 10 years of simulations have been conducted for each site. In addition, in three
630 sites different model initializations (i.e. considering different forest structure, composition and
631 cohorts) were used to quantify improvements in model results when a more detailed
632 heterogeneity forest structure representation and processes are simulated. Modelled GPP
633 results were compared against those from EC observations collected for these sites
634 encompassing three mono-specific (pure) stands of Beech, Holm oak and Scots pine, and
635 three uneven-aged, multi-layered and mixed stands.

636 Based on results, we can now provide answers to the four initial questions:

637 ***1. Does the model reproduce the magnitude and timing of seasonal fluctuations in
638 GPP and their effects across different forest types, structures and compositions?***

639 Overall, as desirable, the model is skilful in reproducing the annual GPP and its intra-annual
640 (seasonal) cycle, calculated as both daily and monthly value averages, with the monthly scale
641 performing better across all statistical indexes considered. These results can be however
642 considered as a “false positive” due to the strong seasonality of GPP patterns that influences
643 and causes higher values of correlation than the model’s capabilities to reproduce GPP fluxes
644 (Zhao et al., 2012). This is clearly related to the tendency to linearize the relationship among
645 CO₂ flux and PAR and/or temperature, as also reported by Ruimy et al. (1995) and Wu et al.
646 (2015). Overall, statistical indexes of daily and monthly modelled values for both X and Y
647 datasets were highly consistent with EC data, except for the Mediterranean sites (where
648 seasonality is less pronounced) (see Table S1a and b). Summer drought stress appeared to be
649 the most limiting factor on photosynthesis at FR-Pue (Falge et al., 2002; Reichstein et al.,
650 2002; Sabatè et al., 2002) while the presence of shallow groundwater table at IT-Cpz seemed
651 to reduce the severity of summer drought. This reduction cause a smoothing of seasonality
652 well highlighted in the Y dataset (see Table S1-b) where IT-Cpz showed to be unanimously
653 one of the worst simulated site at both daily and monthly timescale while FR-Pue and DE-
654 Tha, both evergreens, the less affected by seasonal patterns. This behaviour is confirmed by
655 the daily values of DK-Sor and IT-Col for monthly data, both deciduous, that showed to be
656 the most affected, in other words if we smooth over the seasonal trends results get worse
657 while the model indicated to be less sensitive for those evergreen sites where seasonality is
658 not marked with high values of correlation for DE-Tha, FI-Hyy and Fr-Pue. These results
659 confirm that seasonality has a remarkable effects on a model evaluation.

660 Concerning the seasonality, all statistical indexes divided by seasons in Table S2 are
661 consistent in showing a non-negligible uncertainties in representing GPP patterns, as well as
662 inferred by temporal mismatches in variance. The overall agreement despite temporal
663 mismatches suggested that errors compensated over the year, but are cumulated in specific
664 time windows (e.g. seasons). As reported for other models (Morales et al., 2005 and Naudts et
665 al., 2014), the model's performances are generally worse in winter (DJF) and summer (JJA).
666 Biases and differences in winter GPP variance may be related, among other things, to the
667 model algorithms used to simulate LAI and to the algorithm used to calculate GPP from EC
668 data (Reichstein et al., 2005), since GPP variability should be low during DJF or absent for
669 deciduous forests. However, mismatches are also related to the way in which 3D-CMCC
670 FEM represents winter and early spring ecosystem processes. The model in fact does not
671 consider the influence of ground vegetation that appears to be not negligible in some cases
672 (Kolari et al., 2006). High GPP variance for evergreen species could be strongly related to
673 low temperatures during winter (Del Pierre et al., 2009). Systematic overestimation in winter
674 and spring GPP could then be associated with a lack in representing conifers acclimation or to
675 soil and atmosphere thermal constraints. At high latitudes and altitudes, another source of
676 uncertainty may be related to freezing and thawing dynamics in soil water (Beer et al., 2007)
677 which are not considered by the model, as with snow sublimation and melting, which are still
678 simplistically represented.

679 GPP of deciduous forests in summer and autumn are also affected by uncertainties for
680 surface, which is represented by LAI in the model. In addition, GPP is linear with respect to
681 PAR (Monteith, 1977) over monthly or annual time scales, while the relation is strongly
682 nonlinear at the daily scale (Leuning et al., 1995; Gu et al., 2002; Turner et al., 2003; Wu et
683 al., 2015). The linear response of GPP to PAR led to the underestimation/overestimation of
684 GPP under conditions of low/high incident PAR (Propastin et al., 2012; He et al., 2013). In
685 the case of stress or photoinhibition, leaves reduce or stop photosynthesis at too high levels of
686 radiation, while in normal conditions, photosynthesis is light-saturated at high PAR (Mäkelä
687 et al., 2008) which lets canopy photosynthesis saturate at relatively low PAR even in dense
688 tropical forests with high LAI (Ibrom et al., 2008). The model overestimation of summer GPP
689 may thus be partially related to the lack of representation of the canopy photosynthesis
690 saturation processes.

691 Although adopting a more complex phenology scheme in the comparison between deciduous
692 and evergreen forests, our model showed better performances for deciduous compared to
693 evergreen forests. This behaviour is due to the strong seasonality patterns that the deciduous
694 species show, which is consistent with the findings of Zhao et al. (2012) at the two french
695 sites, but contrasts to the results of Morales et al. (2005) who showed that it is generally easier
696 for models to simulate evergreen forests due to the simpler phenology. The present results for
697 evergreen forests are, however, highly affected by the low model performances for the two
698 evergreen Mediterranean forests. As previously stated, overestimation during summer at FR-
699 Pue, and during winter and spring for IT-Cpz, are mostly related to neglecting species-
700 specific drought stress response functions. As in Landsberg & Waring (1997), the water
701 modifier is only based on soil physical characteristics and no consideration is given to the
702 stress tolerance or strategy of the species (Larcher, 2003), suggesting that further model
703 developments should focus on this aspect.

704 Other discrepancies affecting other sites could probably be reduced with a site-specific
705 parameterization.

706 **2. *Does the model reproduce the observed inter-monthly and inter-annual GPP
707 variability?***

708 Overall, the distribution of the modelled inter-monthly variability was sufficiently consistent
709 with the observed one. The model, however, showed reduced variability in the distribution for
710 both conifers and deciduous species. The model's ability in better representing higher rather
711 than lower anomalies suggests that it may still be less sensitive to some drivers of variability.
712 In this context, the phenological cycle may have an important role, since it influences canopy
713 cover and is controlled by environmental drivers (Richardson et al., 2010). According to Suni
714 et al. (2003) and Jeong et al. (2013), spring phenology largely affects the summertime carbon
715 budget. Hence, uncertainties in the growing season start date may affect 3D-CMCC FEM's
716 ability to reproduce IMV. In summer and autumn, petioles loss of turgor, cavitation in xylem
717 vessels and leaf yellowing may have an important role in the GPP variability of temperate
718 forests (Reichstein et al., 2007).

719 Even though evergreen forests do not experience complete dormancy in winter, changes in
720 'greenness' can be attributed to seasonal variation in canopy biochemistry, the production of
721 new foliage by canopy species and, particularly where the overstorey is sparse, the phenology
722 of understory vegetation (Richardson et al., 2010). Leaves of different ages have different

723 efficiency, sensitivity to solar radiation, temperature and water related stresses (Chabot &
724 Hicks, 1982). All these elements may have an important role in affecting GPP dynamics, but
725 are still scarcely or not represented by mechanistic ecosystem or forest models. As a
726 confirmation of these suspects, slight modifications in representing phenology and leaf
727 turnover resulted in general improvement of model consistency with EC data (Marconi,
728 2014).

729 Distribution of IMV values showed specific patterns attributable to the dominant species.
730 Beech forests IMV PDFs were concentrated around the average value and strongly influenced
731 by high biases. This pattern was probably due to the fact that half of the months in one year
732 have no or little photosynthesis (i.e. early spring, fall and winter) and most of the
733 photosynthetic activity occurs in late spring and summer, when carbon assimilation is
734 influenced by temperatures and solar radiation (Mercado, et al.; 2009). Conifers PDFs were
735 usually smoother, non-skewed, with reduced variability and fitted by a statistical normal
736 curve. The model showed an average NRMSE for IMV of 1.22 but still captured about two
737 thirds of the annual anomalies sign (a little bit more than the fifty percent that represents a
738 simple causality).

739 The results for IAV (see Figure 9) are quite contrasting and largely depend on the site and the
740 number of annual-by-annual comparisons. The recent modelling studies, that we are aware,
741 show unanimously the difficulties of models to explain the large interannual variability in
742 cases where no obvious triggers like management or climatic extreme are at work (e.g.
743 Keenan et al., 2012; Wu et al., 2013). In 3D-CMCC FEM better results have been obtained
744 for FI-Hyy and FR-Pue, so there is no apparent correlation with latitudes and forest species.
745 Interestingly, the performance of a DGVM for IAV in FR-Pue is also higher than other sites
746 (Zhao et al., 2012), indicating the main determinant factor for GPP simulation in this
747 Mediterranean site may not come from the treatment of canopy representation. However, the
748 advantage of a 3D canopy representation needs to be revalued in the future. Similarly, worse
749 results are reported for IT-Ren, IT-Cpz and BE-Bra where the number of annual correlations
750 are lower than the other sites. The magnitude of differences in the standard deviation
751 generally follows the same tendency, particularly for BE-Bra, IT-Ren and IT-Cpz. These
752 results confirm the model's limited ability to represents the inter-annual variability in these
753 specific sites rather than in these ecosystems.

754 The comparison between modelled and observed data at the inter-annual time scale shows the
755 model to be sufficiently able to reproduce the sign of variability through the years including
756 the extreme events (heat wave combined to drought) during the summer 2003 (Ciais et al.,
757 2005; Vetter et al., 2008) and, for some sites, the anomalous carbon uptake during the warm
758 spring of 2007 described by Del Pierre et al. (2009). Potentially negative effects from the
759 anomalous 2003 were modelled into negative GPP anomaly at DK-Sor and IT-Cpz due to
760 model simulation of summer drought stress, while such anomalies are not evident from
761 measurements for DK-Sor (Pilegaard et al., 2011) and IT-Cpz. This could be due to the more
762 maritime climate for DK-Sor and the presence of shallow groundwater for IT-Cpz that
763 weakened the effects in the first part of the summer. In both sites, and included DE-Tha, the
764 effects during July to September were captured by the model (data not shown). As reported by
765 Ciais et al. (2005), Mediterranean sites showed a smaller degree in carbon fluxes, largely
766 dominated by less respiration. It is noteworthy that IT-Col, differently from other european
767 beech stands, does not seems to have suffered from this anomalous heat wave in 2003 (G.
768 Matteucci, personal communication). Both simulated and observed data showed a positive
769 GPP anomaly, demonstrating that this beech forest benefited by moderate higher temperature
770 values and consequently had “extra” days for assimilation and growth (see also Churkina et
771 al., 2002; Richardson et al., 2010). A similar behaviour was reported also by Jolly et al.
772 (2005) for the Swiss Alps, especially between March and July. This pattern seems to be
773 mostly related to an untimely beginning of the growing season (see Piao et al., 2006), to a
774 reduction in plant transpiration that causes an increase in plant water use efficiency through
775 the partial closure of stomata (Warren et al., 2011) and to high fluxes related to forest floor
776 vegetation.

777 It is also noticeable that in FR-Hes during the summer of 2004 a negative anomaly occurred,
778 larger than in 2003; and while its sign was captured by the model, its magnitude was not. This
779 can be explained by the modelled postponed effects of a low NSC allocation during the year
780 2003 to the subsequent periods (Granier et al., 2007; Gough et al., 2009). These results
781 highlight that model has a sort of “memory” linked to short-term events (e.g. drought stress)
782 and that these events affect the long-term processes.

783 Quantitatively, modelled inter-annual anomalies show a very large spread across the sites.
784 Correlations vary widely, without any apparent relation with latitude and/or species. If
785 modelled anomaly signs are potentially agreeing with the observed ones most of the time,

786 their magnitude was not. This behaviour seems to be related to several aspects, mainly to an
787 over/under estimation of the causes that reproduce anomalies, e.g. processes simulated linked
788 to the type of climate anomaly, mismatches in phenology or to a missed representation of
789 other processes (e.g. mast years, disturbances, shallow water). Keenan et al. (2012) asserts
790 that a lack in phenological variability and in canopy and soil dynamics are the main culprits of
791 these mismatches but also that flux measurements are affected by random errors especially
792 when fluxes are higher. Poulter et al. (2009) found a similar magnitude of errors with models
793 that were driven by remote-sensing data. Open questions remain as to the proportion of
794 interannual variability in land-atmosphere carbon exchange that is directly explainable by
795 variability in climate (Hui et al., 2003; Richardson et al., 2007)

796 ***3. Is the model generic enough that a single set of species-specific parameterization
797 allows reproducing GPP behaviour across different ecosystems without further need of a
798 site-related calibration?***

799 Overall, the model showed good flexibility although the sites showed a pronounced spatial
800 and temporal heterogeneity (i.e. a variable number of forest layers, different cohorts and
801 species). The model was able to reliably represent the ecophysiology of beech and spruce
802 species at different latitudes, without modifying or tuning the parameterization sets. However,
803 annual and seasonal performance indices, calculated exploiting daily and monthly series,
804 evidenced different performances between the two northern beech sites and the two southern
805 ones. Tables S1 and S2 show a systematic difference in all the statistics used, suggesting the
806 presence of a latitudinal gradient in 3D-CMCC FEM's ability to represent beech forest
807 processes. This gradient could be explained by how the model represents the different limiting
808 factors and their impacts on GPP. For example, we expect low temperatures to be the most
809 important limiting factor at higher latitudes, compared to soil water availability at lower
810 latitudes (Chapin et al., 2002).

811 We obtained similar results for the two spruce sites. The model showed better performance at
812 higher latitudes. While phenotypic plasticity, and thus the parameter set, may influence the
813 model results, it is noteworthy that the IT-Ren site has different topographic and climatic
814 conditions. Lower average temperatures, higher slopes, and non-negligible encroachment of
815 different species in a more complex canopy, may negatively influence the model performance
816 in IT-Ren with respect to DE-Tha. Since the model showed unrealistic results for the two
817 Mediterranean forests, we think it is not easy to determine if and how differences in

818 performances are related to the generality of the model rather than to bad assumptions behind
819 the simulated processes. From our findings, we conclude that for non-water limited conditions
820 it is possible to yield satisfying results with general parameter sets.

821 **4. *Do the model's results improve when considering a complex 3D canopy structure?***

822 We evaluated possible improvements that could be made if a more accurate model
823 representation at a higher rate of heterogeneity of: forest structure, differences in ages and
824 species composition and their linked structural-ecophysiological processes, are assumed.
825 These analyses helped us to understand the importance of each process within the represented
826 combination (i.e. light competition, age related decline and the specific differences in
827 ecophysiology) on modelled GPP. Doubtless, a direct comparison between modelled and
828 observed GPP data is not possible due to the lack of partitioned measurements of GPP across
829 different layers, cohorts and species. However, in situations where the different
830 ecophysiological behaviours express themselves in the species specific canopy responses
831 during certain periods of the seasonal cycle, the test of a mixed forest tree model with flux
832 measurements is possible, as the results by Oltchev et al. (2002) showed using the model
833 MixFor-SVAT.

834 This preliminary analysis can be considered as a sensitivity analysis in terms of processes
835 explicitly simulated instead of lumped parameterisation. As a whole, model results using
836 different initialization data are within the observed GPP uncertainties but a quantitative
837 assessment for two sites, BE-Bra and IT-Ren showed the potential to increase the model's
838 ability in simulating fluxes, while for DE-Tha there is no evidence that model performances
839 could benefit of these efforts. For BE-Bra, taking into account two species (that differ
840 especially for their phenological traits) was beneficial in terms of model performances, the
841 same occurred for different layers (with the exception of BE-Bra P_Q-3L vs. BE-Bra P_Q-2L
842 whose results were similar) and different cohorts. Better performances, in terms of seasonal
843 GPP representations, were obtained when each of the above mentioned characteristics was
844 accounted for by the model. For IT-Ren, similar results were obtained, although no
845 differences were found in the simulation of phenological patterns in daily and monthly results.
846 Differently, for DE-Tha a differentiation between the two evergreen coniferous species did
847 not cause marked differences in model results, due to low differences in species
848 ecophysiological traits, justifying in these cases the use of a Plant Functional Type (PFT)
849 level of parameterization instead species level (Poulter et al., 2015).

850 **5 Conclusions**

851 This study aimed at evaluating the performances of the updated version of 3D-CMCC FEM
852 compared to nearly 10x10 sites x years GPP data across eddy-covariance European forest
853 sites. Although the sites showed high spatial and temporal environmental heterogeneity the
854 model appears able to reproduce trends in all of the ten sites. Different performance indexes
855 showed that daily and monthly level model results match well, both for the annual and
856 seasonal scale, against observed data, with some exceptions. Mediterranean sites (IT-Cpz and
857 FR-Pue) showed to be the most problematic in reproducing carbon fluxes. This is likely due
858 to their specific ecosystem peculiarity, e.g. shallow groundwater for IT-Cpz and, for both
859 sites, a low pronounced seasonality. In these two sites, the model showed less generalisation
860 unless additional processes were included. Differently from other models, 3D-CMCC FEM,
861 both for daily and monthly simulations and for both X and Y datasets, performs better for
862 deciduous species rather than for evergreen, although deciduous species have a more complex
863 phenology and a more pronounced seasonality. Some mismatches in the simulation over the
864 seasons and over the sites still remain, especially during winter and summer. The first reason
865 for these low agreements in winter can be also attributable to errors during the estimation of
866 GPP from NEE and Ecosystem Respiration values from measurements data. The second can
867 be related to the model's lack or simplicity in representation of snow pack dynamics as
868 reported by Krishnan et al. (2008; 2009), especially for evergreen sites (Keenan et al., 2012).
869 Disagreements in summer could be related to model simplicity in simulating soil drought and,
870 using the Monteith approach (Monteith, 1977), to the strong nonlinearity at the daily scale of
871 GPP and PAR, and to the lack of representation of the light saturation processes. In addition,
872 as reported by Keenan et al. (2012), the apparent high variability in the data during the
873 summer season could therefore be due to random errors in the flux measurements, generating
874 larger variability and then lower correlations against modelled data.

875 No marked differences were found in simulations across different latitudes, so model
876 parameterizations for the different tree species could be useful over Europe with quite a high
877 rate of confidence, with the exception of specific cases in Mediterranean forests.

878 As for other models, 3D-CMCC FEM showed to have the potential to correctly reproduce the
879 signs of interannual variability, like the 2003 heat wave and drought extreme and the
880 anomalous carbon uptake during the warm spring of 2007 and their instantaneous biological

881 response to these events. Significant disagreements were, however, found in reproducing the
882 magnitude of these anomalies.

883 The consideration of stand heterogeneity, when possible or existing (i.e. layers, cohorts and
884 mixed composition), led the model to improve its results in two of the three sites compared to
885 generalized simulations of forest attributes. This plasticity makes the model able to be used in
886 a wider range of forest ecosystems.

887

888 **Author contribution**

889 A.C. conceived the paper, designed the experiments, co-developed the model code, performed
890 the simulations, and wrote the manuscript with contribution from all co-authors

891 S.M. co-developed the model code, performed the simulations, and contributed to data
892 analysis

893 A.I. contributed to manuscript improvement

894 C.T. contributed to data analysis

895 A.A. contributed to data analysis and to the manuscript improvement

896 E.A. contributed to data analysis

897 G.M. contributed to manuscript improvement and data analysis

898 L.M. contributed to manuscript improvement and data analysis

899 B.G. contributed to manuscript improvement and data analysis

900 I.M. contributed to manuscript improvement and data analysis

901 T.G. contributed to manuscript improvement and data analysis

902 A.K. contributed to manuscript improvement and data analysis

903 F.B contributed to manuscript improvement and data analysis

904 Y.Z. contributed to data analysis and to the manuscript improvement

905 R.V. contributed to manuscript improvements.

906 M.S. contributed to manuscript conceiving and data analysis improvements

907

908 **Acknowledgements**

909 As Euro-Mediterranean Center on Climate Change Foundation and University of Tuscia, we
910 acknowledge project funding by the Italian Ministry of Education, University and Research
911 (MIUR) through the projects GEMINA and CARBOTREES, respectively. Authors are
912 indebted to Dario Papale, Julia McCarrol, J. Curiel Yuste and to the two anonymous
913 reviewers for their useful comments and advises.

914

915 **Table captions**

916 **Table 1** Main characteristics of the study sites. Sites were classified according to the IGBP
917 (International Geosphere Biosphere Program) legend as in the FLUXNET database:
918 MF=mixed forest; DBF=deciduous broadleaf forest; EBF=evergreen broadleaf forest;
919 ENF=evergreen needle leaf forest. Year of simulation starting and ending depend on available
920 time series of observed data.

921 **Table 2** IMV and IAV NRMSE for the analyzed sites. Each specific IMV distribution was
922 tested for normality goodness of fit (N = normal distribution, P = non normal distribution). A
923 test for equivalence of central tendency was performed between IMV_{MD} and IMV_{EC} values.
924 (na) refers to the case of sites with inconsistent distributions (one normally, one not normally
925 distributed). (*) marks refer to the acceptance of the null hypothesis that the two distributions
926 are equivalent for the specific statistic ($\alpha=0.05$). ECT stands for “Equivalence for Central
927 Tendency”; EV for “Equivalence for Variance”.

928 **Table 3** Performance statistics (r, NRMSE, MEF, MABstd) are reported as derived from daily
929 and monthly series of GPP_{EC} and GPP_{MD} values over long-term annual scale, for the different
930 forest structure simulations. The (*) refers to p -value < 0.0001 in correlation between GPP_{EC}
931 and GPP_{MD} data. In addition, long term average of annual GPP_{MD} and GPP_{EC} values ($gC\ m^{-2}$
932 yr^{-1}) for the different forest structures are shown.

933

934

935

936

937

938

939

940

941

942

943

944

945 **Figure captions**

946 **Figure 1** 3D-CMCC FEM performance indices at different time scales; daily (Figure 1-a) and
947 daily aggregated to month (Figure 1-b) for X dataset. Figure 1-c and 1-d refer to Y daily and
948 Y monthly dataset following decomposition technique proposed in Zhao et al. (2012). DE-
949 Tha refers to the 1S simulation, IT-Ren to the 2L_2C simulation, BE-Bra to the P_Q-3L
950 simulation (see text).

951 **Figure 2** Taylor diagrams for daily (a) and daily aggregated to month (b) GPP evaluated
952 representing: the deviation of model results from observations in terms of normalized
953 standard deviation of observations, represented by the distance from the site point to the point
954 on the x-axis identified as reference (REF); the difference of model normalized standard
955 deviation from that of observations, represented by the distance of the site point with respect
956 to the quarter arc crossing REF; and the correlation, given by the azimuthal position of the
957 site point to the x-axis. The sites are numbered in ascending order as follows: (1) DE-Hai, (2)
958 DK-Sor, (3) FR-Hes, (4) IT-Col, (5) FR-Pue, (6) IT-Cpz, (7) DE-Tha, (8) FI-Hyy, (9) IT-Ren,
959 (10) BE-Bra. Colors refer to different IGBP vegetation classes: DBF (yellow), EBF (orange),
960 ENF (light-blue), MF (green).

961 **Figure 3** Distributions of annual GPP ($\text{gC m}^{-2} \text{ yr}^{-1}$). MD (red) are model results, EC (blue)
962 measured by eddy covariance. The vertical bars represent ± 1 standard deviation. DE-Tha
963 refers to the 1S simulation, IT-Ren to the 2L_2C simulation, BE-Bra to the P_Q-3L
964 simulation (see text).

965 **Figure 4** 3D-CMCC FEM performances indices of daily GPP at different seasons. DE-Tha
966 refers to the 1S simulation, IT-Ren to the 2L_2C simulation, BE-Bra to the P_Q-3L
967 simulation (see text).

968 **Figure 5** 3D-CMCC FEM performances indices of daily GPP aggregated to months at
969 different seasons. DE-Tha refers to the 1S simulation, IT-Ren to the 2L_2C simulation, BE-
970 Bra to the P_Q-3L simulation (see text).

971 **Figure 6** Comparison between GPP_{MD} and GPP_{EC} data. The top plots show the average
972 $\text{GPP}_{\text{EC}}:\text{GPP}_{\text{MD}}$ correlation for (left) monthly ($\text{gC m}^{-2} \text{ month}^{-1}$) and (right) daily ($\text{gC m}^{-2} \text{ d}^{-1}$)
973 data. The bottom plots show absolute difference range between GPP_{MD} and GPP_{EC} while
974 increasing GPP_{EC} values. Negative values are excluded because of model assumptions. DE-

975 Tha refers to the 1S simulation, IT-Ren to the 2L_2C simulation, BE-Bra to the P_Q-3L
976 simulation (see text).

977 **Figure 7** Seasonal (monthly) cycle of GPP across the ten sites. The grey line and margins of
978 the grey area represent long-term average of monthly GPP_{EC} ($\text{gCm}^{-2}\text{month}^{-1}$) and its ± 1
979 standard deviation, respectively. The green and red dashed lines represent the long-term
980 average of monthly GPP_{MD} ($\text{gCm}^{-2}\text{month}^{-1}$) and its ± 1 standard deviation, respectively. DE-
981 Tha refers to the 1S simulation, IT-Ren to the 2L_2C simulation, BE-Bra to the P_Q-3L
982 simulation (see text).

983 **Figure 8** Distribution of the magnitude for the inter-monthly variability values (IMVs, $\text{gC m}^{-2}\text{d}^{-1}$) for each specific site, resulted by standard kernel density estimation. The vertical red line
984 is the media, the box plot limit the 25th and 75th percentiles, the dashed black bars represent
985 the rest of the distribution range excluding outliers (red crosses) DE-Tha refers to the 1S
986 simulation, IT-Ren to the 2L_2C simulation, BE-Bra to the P_Q-3L simulation (see text).

987 **Figure 9** Inter-Annual Variability (IAV) based on Keenan et al. (2012). Red and blue bars
988 indicate the observed and modelled IAV values, respectively; r values refer to correlation
989 between observed and modelled variations. DE-Tha refers to the 1S simulation, IT-Ren to the
990 2L_2C simulation, BE-Bra to the P_Q-3L simulation (see text).

1 Table 1.

Site Name (Site code)	Lat (°) / Lon (°)	IGBP	Simulation year (Starting - Ending)	Mean Annual Temperature (°C)	Annual Precipitation Amount (mm yr ⁻¹)	Elevation (m a.s.l.)	Main species and forest description	Main references
Hainich (DE-Hai)	51.08 / 10.45	DBF	2000 – 2007	8.3	720	445	Uneven-aged, unmanaged multi-layered forest of beech (<i>Fagus sylvatica</i> , 250 years, mean DBH 30.8 cm, mean tree height 23.1 m, stand density 334 trees/ha)	Knohl et al., 2003 + BADM files
Sorø (DK-Sor)	55.49 / 11.64	DBF	2001 – 2009	8.2	660	40	Beech (<i>Fagus sylvatica</i> , averagely 80 years, mean DBH 36.13 cm, mean tree height 25 m, stand density 283 trees/ha)	Pilegaard et al., 2003 + BADM files
Hesse (FR-Hes)	48.67 / 7.07	DBF	2001 – 2007	9.2	820	300	Beech (<i>Fagus sylvatica</i> , averagely 35 years, mean DBH 8.19 cm, mean tree height 13 m, stand density 3384 trees/ha)	Granier et al., 2000 + BADM files
Collelongo (IT-Col)	41.85 / 13.59	DBF	1997 – 2012	6.3	1180	1550	Beech (<i>Fagus sylvatica</i> , averagely 100 years, mean DBH 20.2 cm, mean tree height 19.8 m, stand density 900 trees/ha)	Scartazza et al., 2013 + BADM files
Puechabon (FR-Pue)	43.74 / 3.60	EBF	2000 – 2011	13.5	883	270	Holm oak (<i>Quercus ilex</i> , averagely 59 years, mean DBH 7 cm, mean tree height 6 m, stand density 8500 trees/ha)	Loustau et al., 2005 + BADM files
Castelporziano (IT-Cpz)	41.71 / 12.38	EBF	2000 – 2008	15.6	780	3	Holm oak (<i>Quercus ilex</i> , averagely 45 years, mean DBH 16 cm, average tree height 12.5 m, stand density 458 trees/ha)	Vitale et al., 2003 + BADM files
Tharandt (DE-Tha)	50.96 / 13.57	ENF	2000 – 2010	7.7	820	380	Mixed Norway spruce (<i>Picea abies</i> , averagely 113 years, mean DBH 33 cm, tree height 26, density 396 trees/ha) and Scots Pine (<i>Pinus sylvestris</i> , averagely 113 years, mean DBH 33.1 cm, tree height 26.1 m, density 81 trees/ha)	Grünwald & Bernhofer, 2007 + BADM files
Hyttiälä (FI-Hyy)	61.85 / 24.29	ENF	2001 – 2011	3.8	709	170	Scots pine (<i>Pinus sylvestris</i> , 39 years, mean DBH 30.8 cm, mean tree height 23.1 m, stand density 334 trees/ha)	Suni, et al., 2003 + BADM files

Renon (IT-Ren)	46.59 / 11.43	ENF	2006 - 2010	4.7	809	1735	Uneven-aged multi-layered forest of Norway spruce (<i>Picea abies</i> averagely, 190 and 30 years, average DBH 30.8 cm, average tree height 23.1m, stand density 334 trees/ha)	Montagnani et al.(2009) + BADM files
Brasschaat (BE-Bra)	51.30/4.52	MF	2001 - 2010	9.8	750	16	Mixed, uneven-aged multi-layered forest of Scots pine (<i>Pinus sylvestris</i> , averagely 72 years) and Pedunculate oak (<i>Quercus robur</i> , averagely 65 years)	Gielen et al., 2013 + BADM files

1 *Table 2*

		DE-Hai	DK-Sor	FR-Hes	IT-Col	FR-Pue	IT-Cpz	DE-Tha (1S)	FI-Hyy	IT-Ren (2L-2C)	BE-Bra (P_Q-3L)
NRMSE	IAVs	2.4	1.8	1.3	0.3	0.6	1.1	1.0	2.7	1.3	0.9
NRMSE	IMVs	1.7	2.7	1.1	0.6	1.1	1.2	1.1	1.2	1.0	0.5
ECT	p-value	1.00* ^N	0.12* ^N	0.54* ^N	0.00 ^N	0.15* ^N	1.00* ^{na}	1.00* ^P	0.04 ^N	0.88* ^P	0.85* ^N
EV	p-value	0.53* ^N	0.00 ^N	0.00 ^N	0.46* ^N	0.00 ^N	0.02 ^{na}	0.78* ^P	0.00 ^N	0.27* ^P	0.01 ^N

2

3

1 *Table 3.*

2

Site	Model set-up code	Daily				Monthly				Yearly	
		r	NRMSE	MEF	MABstd	r	NRMSE	MEF	MABstd	GPP _{MD} gC m ⁻² yr ⁻¹	GPP _{EC} gC m ⁻² yr ⁻¹
BE-Bra	P	0.72*	0.73	0.47	0.51	0.86*	0.55	0.70	0.39	1003	
	Q_3L	0.76*	0.91	0.18	0.67	0.84*	0.71	0.49	0.52	1105	
	Q_2L	0.74*	0.89	0.21	0.66	0.86*	0.74	0.45	0.55	1179	
	Q_1L	0.75*	0.95	0.01	0.70	0.86*	0.68	0.53	0.50	1147	
	P_Q- 3L	0.77*	0.65	0.57	0.46	0.93*	0.39	0.84	0.28	1141	1193
	P_Q- 2L	0.75*	0.67	0.55	0.46	0.91*	0.44	0.81	0.30	1037	
	P_Q- 1L	0.75*	0.66	0.56	0.46	0.91*	0.68	0.53	0.50	1056	
IT-Ren	2L_2C	0.82*	0.62	0.61	0.44	0.95*	0.30	0.91	0.23	1349	
	1L_1C	0.83*	0.85	0.27	0.61	0.96*	0.61	0.62	0.45	1950	1362
DE-Tha	1S	0.90*	0.46	0.79	0.31	0.96*	0.27	0.93	0.19	1840	
	2S	0.89*	0.48	0.80	0.31	0.95*	0.29	0.91	0.19	1898	1869

3

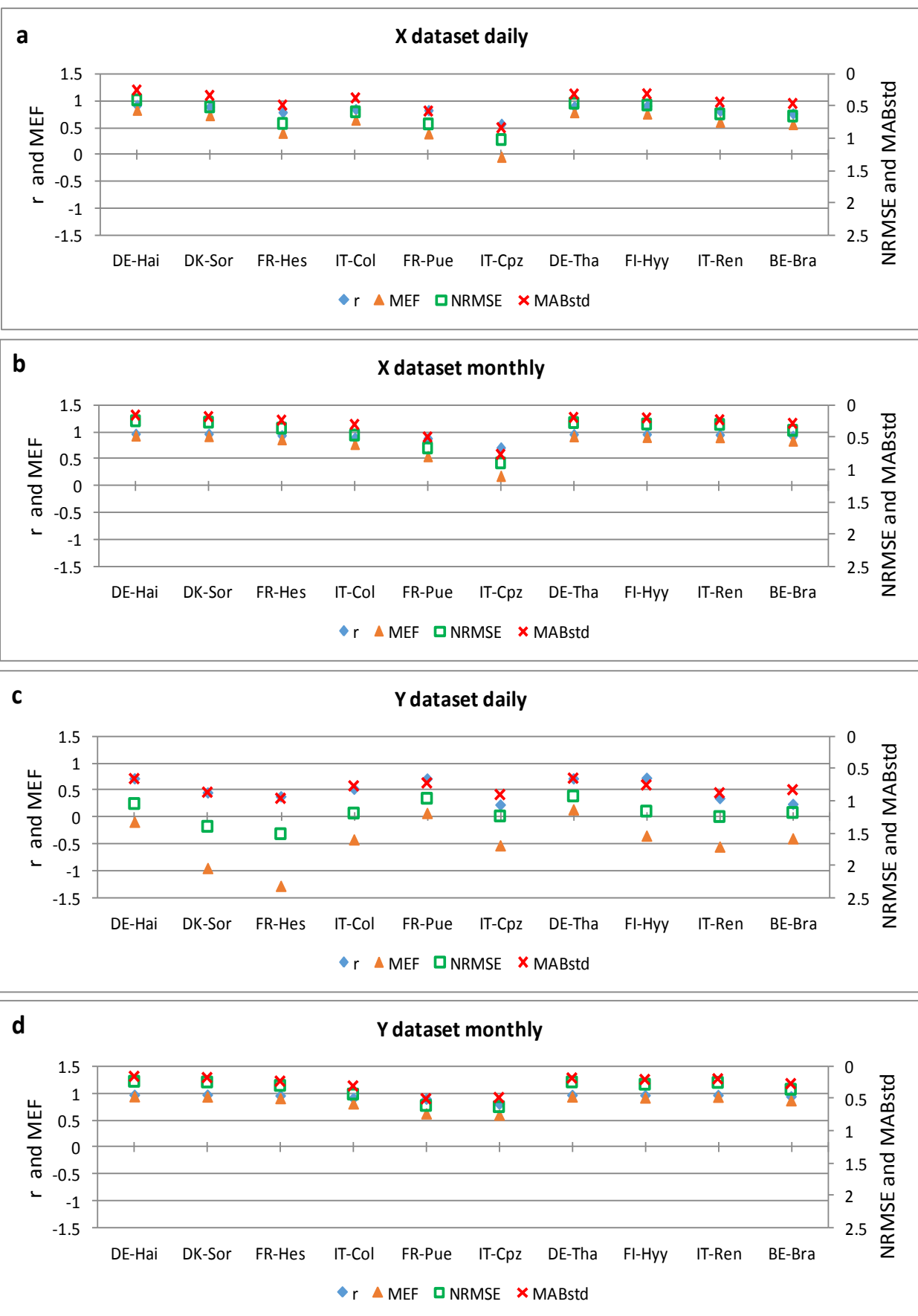
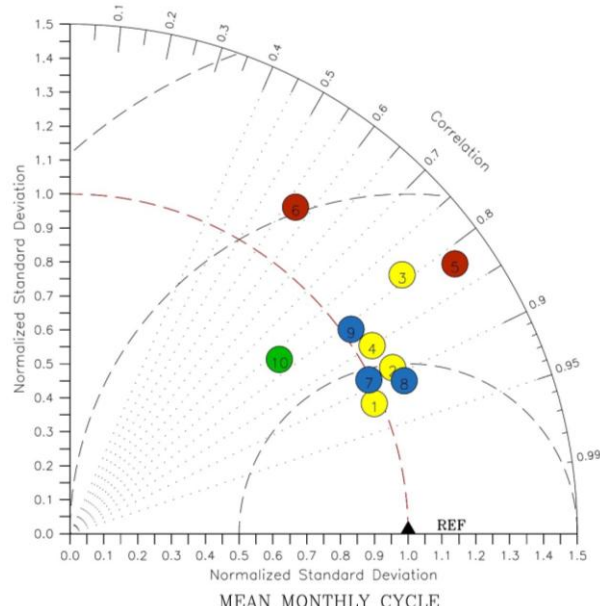


Figure 1

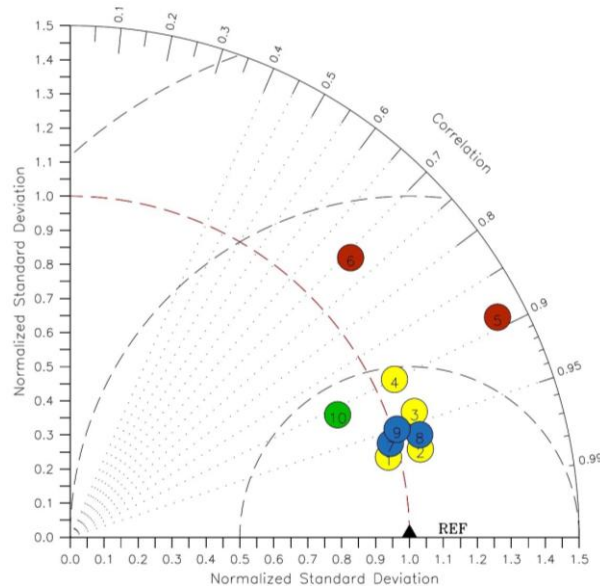
4

MEAN DAILY CYCLE



5

MEAN MONTHLY CYCLE



6

7 *Figure 2*

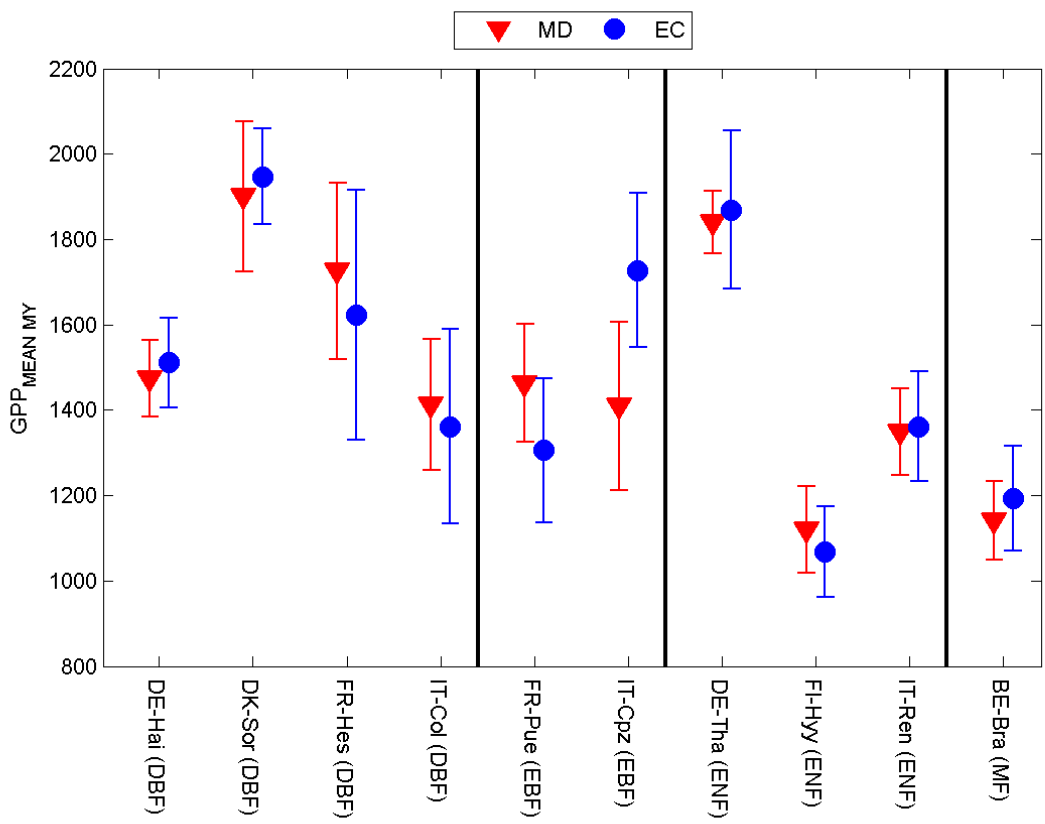


Figure 3

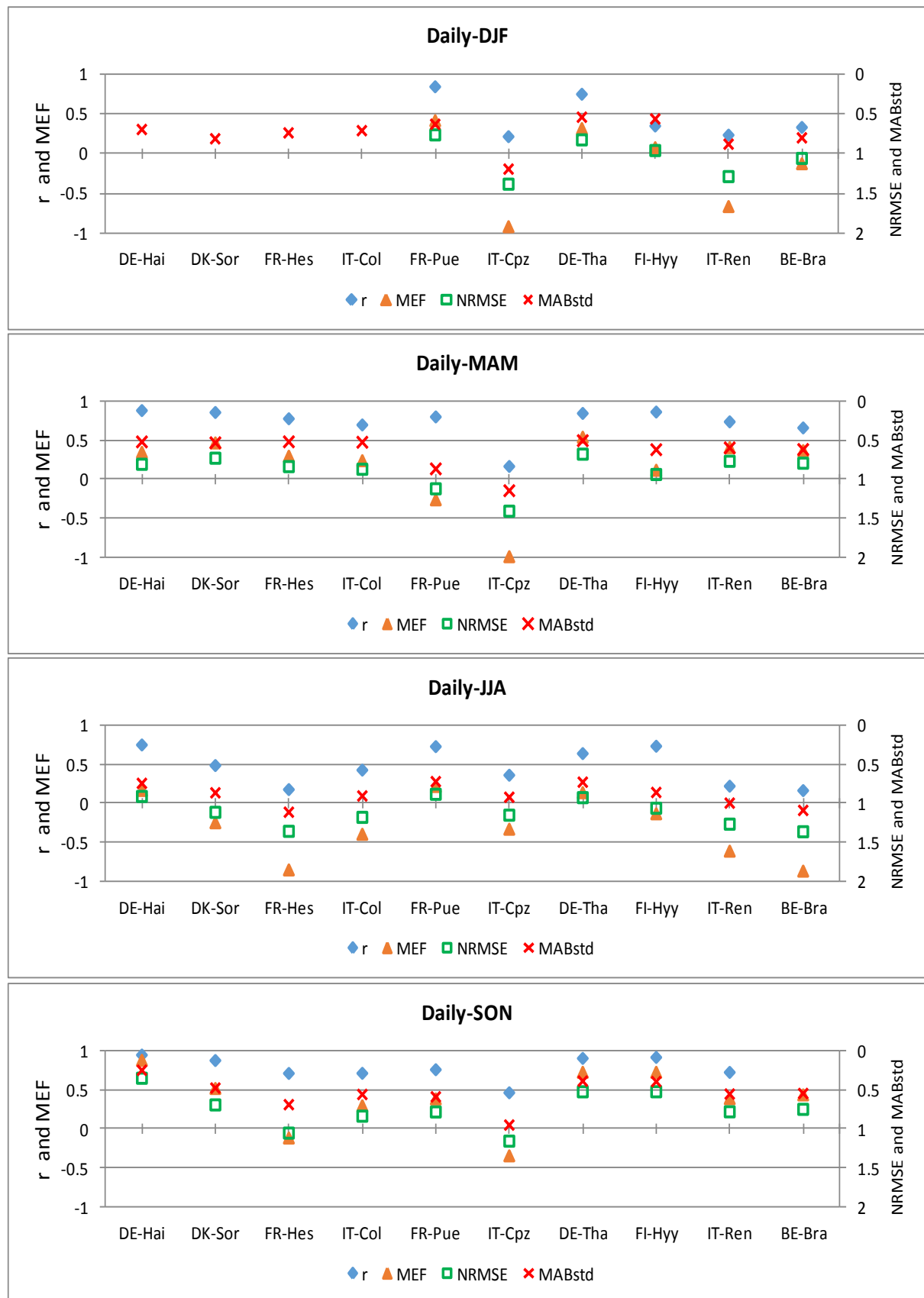


Figure 4

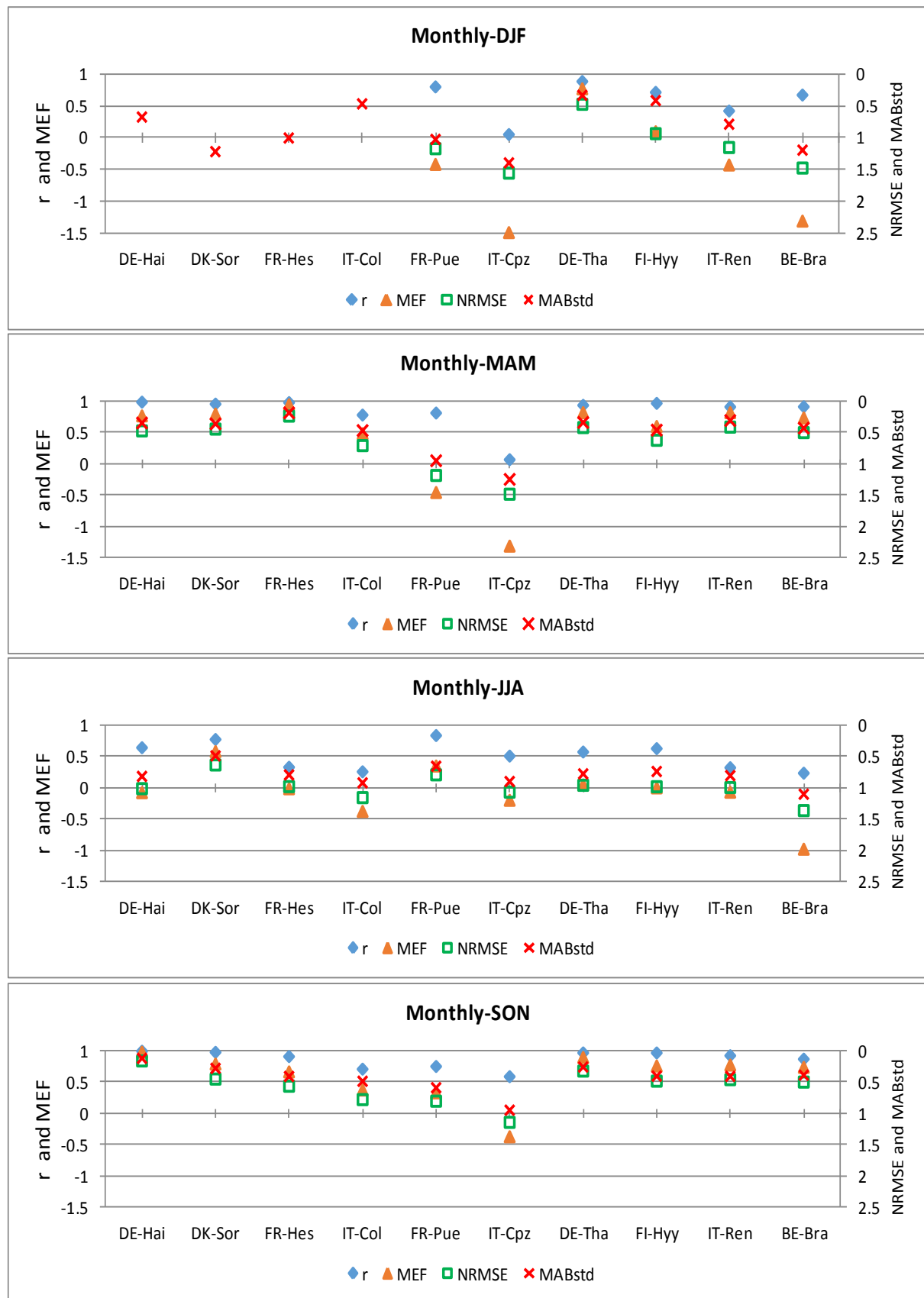
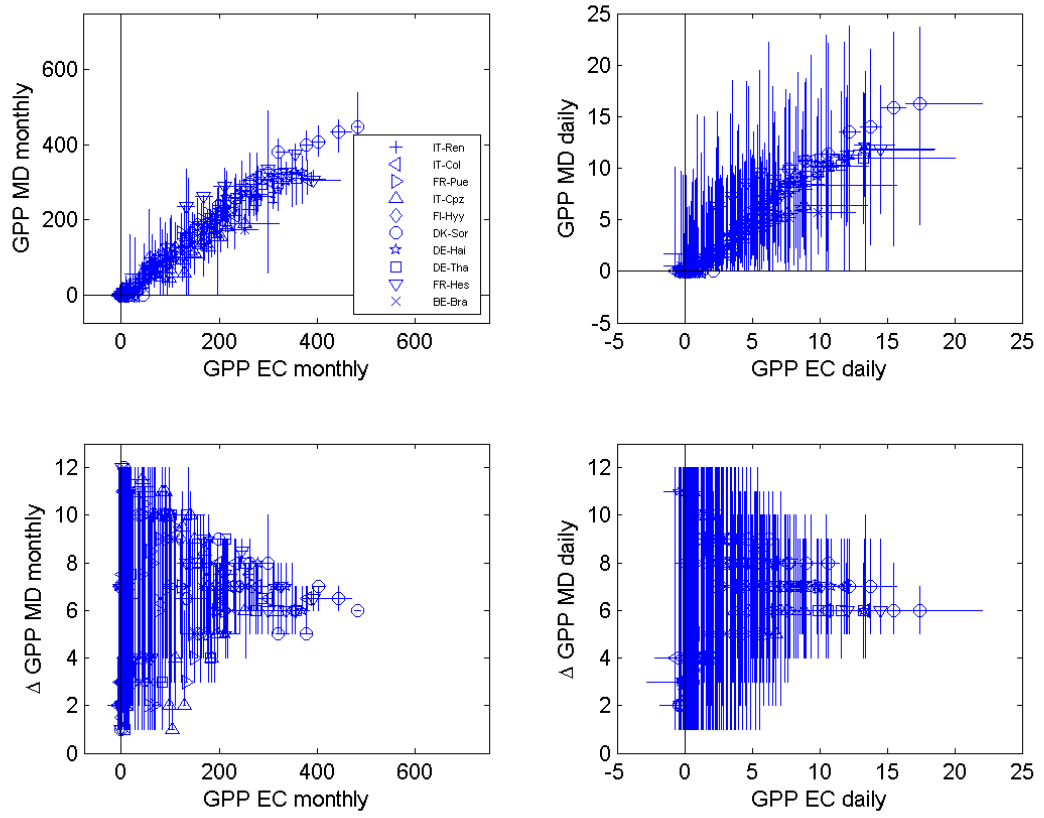


Figure 5



13

14 *Figure 6*

15

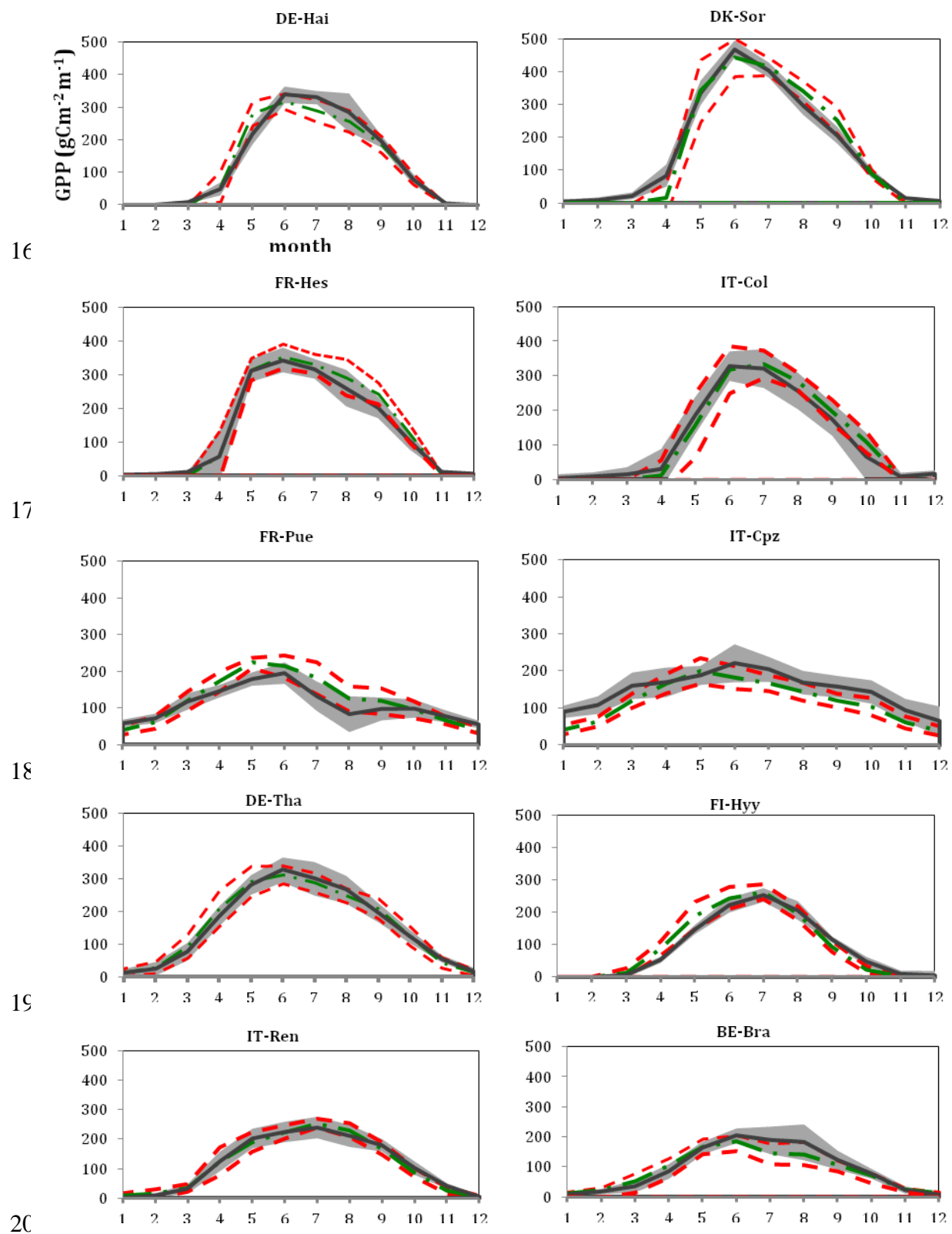
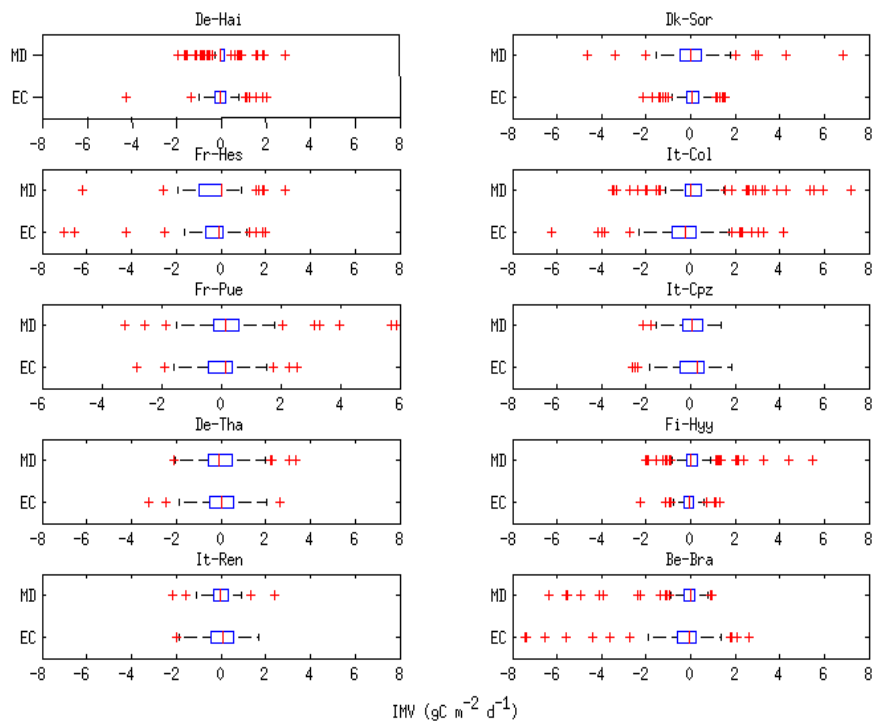


Figure 7

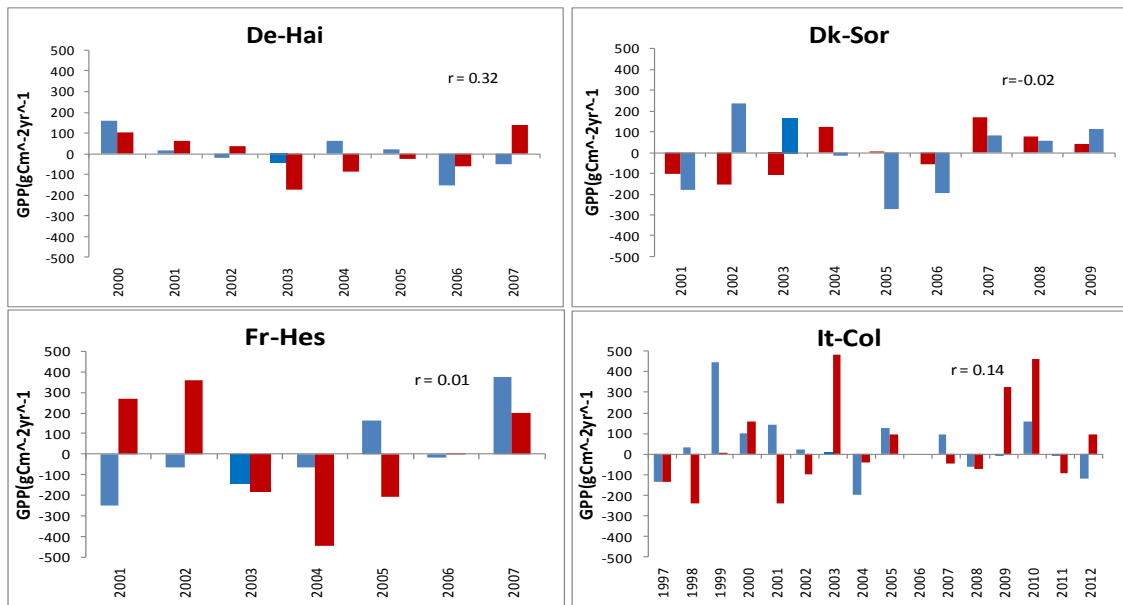


23

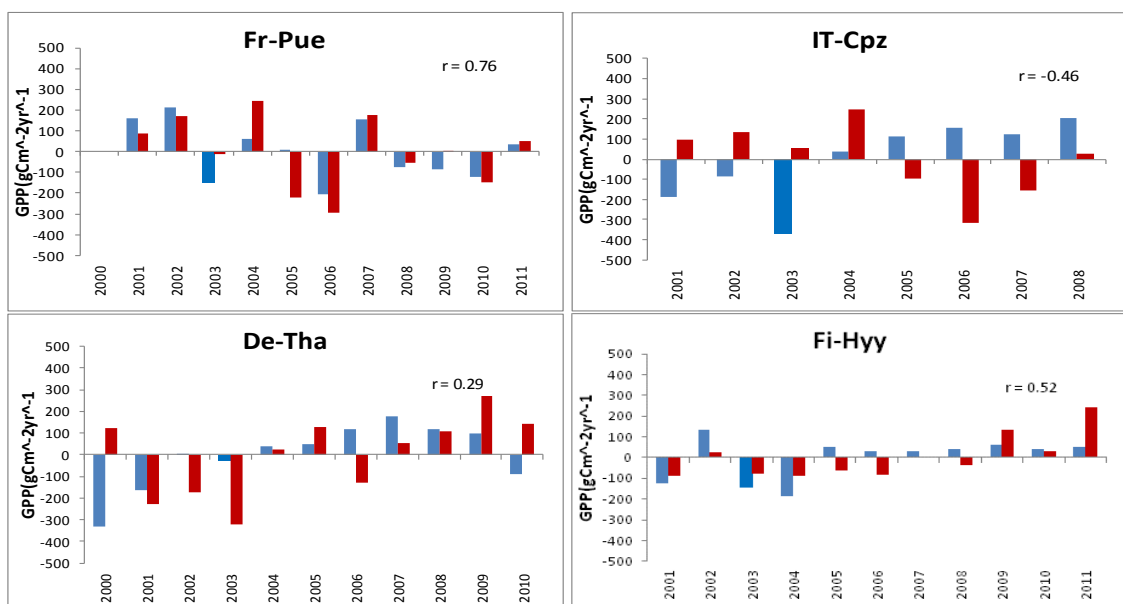
24 *Figure 8*

25

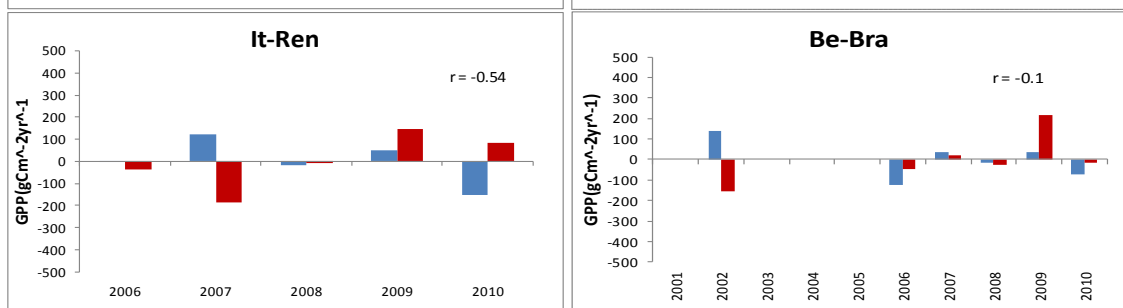
26



27



28



29

31 *Figure 9*

32

33

34 **References**

35 Anav, A., D'Andrea, F., Viovy, N., & Vuichard, N. (2010). A validation of heat and carbon
36 fluxes from high-resolution land surface and regional models. *Journal of Geophysical*
37 *Research* , 115: 1-20.

38 Arneth, A., Sitch, S., Bondeau, A., Butterbach-Bahl, K., Forest, P., Gedney, N., et al. (2010).
39 From biota to chemistry and climate: towards a comprehensive description of trace gas
40 exchange between the biosphere and atmosphere. *BioGeosciences* , 7, 121-149.

41 Arora, V. K., & Boer, G. J. (2005). A parameterization of leaf phenology for the terrestrial
42 ecosystem component of climate models. *Global Change Biology* , 11: 39-59.

43 Aubinet, M., Grelle, A., Ibrom, A., Rannik, U., Moncrieff, J., Foken, T., et al. (2000).
44 Estimates of the annual net carbon and water exchange of European forests: the EUROFLUX
45 methodology. *Advances in Ecological Research* , 30, 113-175.

46 Bagnara, M., Van Oijen, M., Cameron, D., Gianelle, D., Magnani, F., & Sottocornola, M.
47 (2014). A user-friendly forest model with a multiplicative mathematical structure: a Bayesian
48 approach to calibration. *Geosci. Model Dev. Discuss.* , 7, 6997-7031.

49 Baldocchi, D. (2003). Assessing the eddy covariance technique for evaluating carbon dioxide
50 exchange rates of ecosystems: past, present and future. *Global Change Biology* , 9, 479-492.

51 Balzarolo, M., Boussetta, S., Balsamo, G., Beljaars, A., Miagnan, F., Calvet, J.-C., et al.
52 (2014). Evaluating the potential of large-scale simulations to predict carbon fluxes of
53 terrestrial ecosystems over a European Eddy Covariance network. *Biogeosciences* , 11-
54 2661,2678.

55 Barbaroux, B., & Bréda, N. (2002). Contrasting distribution and seasonal dynamics of
56 carbohydrate reserve in stem wood of adult ring-porous sessile oak and diffuse-porous beech
57 trees. *Tree Physiology* , 1201-1210.

58 Batlle Bayer, L., van den Hurk, B., Strengers, B., & van Minnen, J. (2012). Regional
59 feedbacks under changing climate and land-use conditions. *Earth Syst. Dynam. Discuss.* , 3,
60 201-234.

61 Battin, T., Luyssaert, S., Kaplan, L., Aufdenkampe, A., Richter, A., & Tranvik, L. (2009).
62 The boundless carbon cycle . *Nature Geoscience* , 2, 598-600.

63 Beer, C., Reichstein, M., Tomelleri, E., Ciais, P., Jung, M., Carvalhais, N., et al. (2012).
64 Terrestrial Gross Carbon Dioxide Uptake: Global Distribution and Covariation with Climate.
65 *Science* , 329, 834-838.

66 Blyth, E., Clark, D., Ellis, R., Huntingford, C., Los, S., Pryor, M., et al. (2011). A
67 comprehensive set of benchmark tests for a land surface model of simultaneous fluxes of
68 water and carbon at both the global and seasonal scale. *Geosci. Model Dev.* , 4, 255-269.

69 Bolstad, P., Mitchell, K., & Vose, J. (1999). Foliar response functions for broad-leaved tree
70 species in the southern Appalachians. *Tree Physiology* , 19, 871-878.

71 Bonan, G. B. (2008). Forest and Climate Change: Forcings, Feedbacks, and the Climate
72 Benefits of Forests. *Science* , 320, 1444-1449.

73 Bond-Lamberty, B., Gower, S., Ahl, D., & Thornton, P. E. (2005). Reimplementation of the
74 Biome-BGC model to simulate successional change. *Tree Physiology* , 25, 413-424.

75 Bowman, A., & Azzalini, A. (1997). *Applied smoothing techniques for data analysis*. New
76 York: Oxford University Press Inc.

77 Brèda, N., Huc, R., Granier, A., & Dreyer, E. (2006). Temperate forest trees and stands under
78 severe drought: a review of ecophysiological responses, adaptation processes and long-term
79 consequences. *Ann. For. Sci.* , 625-644.

80 Breuer, L., Eckhardt, K., & Frede, H.-G. (2003). Plant parameter values for models in
81 temperate climates. *Ecological Modelling* , 169:237-293.

82 Campioli, M., Verbeeck, H., Van den Bossche, J., Wu, J., Ibrom, A., D'Andrea, E., et al.
83 (2013). Can decision rules simulate carbon allocation for years with contrasting and extreme
84 weather conditions? A case study for three temperate beech forests. *Ecological Modelling* ,
85 263, 42-55.

86 Cescatti, A., Marcolla, B., Santhana, S., & al., e. (2012). Remote sensing of environment
87 intercomparison of MODIS albedo retrievals and in situ measurements across the global
88 FLUXNET network. *Remote Sensing of Environment* , 121, 323-334.

89 Chabot, B. F., & Hicks, D. (1982). The ecology of leaf life spans. . *Annual Review of Ecology*
90 and Systematics , 229-259.

91 Chai, T., & Draxler, R. (2014). Root mean square error (RMSE) or mean absolute error
92 (MAE)? - Arguments against avoiding RMSE in the literature. *Geosci. Model Dev.* , 7, 1247-
93 1250.

94 Chang, J., Viovy, N., Vuichard, N., Ciais, P., Wang, T., Cozic, A., et al. (2013). Incorporating
95 grassland management in ORCHIDEE: model description and evaluation at 11 eddy-
96 covariance sites in Europe. *Geosci. Model Dev.* , 6, 2165-2181.

97 Chapin, F., Matson, P., & Vitousek, P. (2002). *Principles of Terrestrial Ecosystem Ecology*.
98 New York, NY, USA: Springer.

99 Chesson, P. (2000). Mechanism of maintenance of species diversity. *Annu. Rev. Ecol. Syst.* ,
100 31, 343-366.

101 Churkina, G., Schimel, D., Braswell, B., & Xiao, X. (2002). Spatial analysis of growing
102 season length control over net ecosystem exchange. *Gobal Change Biology* , 11, 1777-1787.

103 Ciais, P., Reichstein, M., Viovy, N., Granier, A., Ogée, J., Allard, V., et al. (2005). Europe-
104 wide reduction in primary productivity caused by the heat and drought in 2003. *Nature* , 437:
105 529-533.

106 Ciais, P., Sabine, C., Bala, G., Bopp, L., Brovkin, V., Canadell, J., et al. (2013). Carbon and
107 Other Biogeochemical Cycles. In T. Stocker, D. Qin, G. -K. Plattner, M. Tignor, S. Allen, J.
108 Boschung, et al., *Climate Change 2013: The Physical Science Basis, Contribution of Working
109 Group I to the Fifth Assessment Report of the Intergovernmental Panel on Climate Change*.
110 Cambridge, United Kingdom and New York, NY, USA: Cambridge University Press.

111 Clark, D., Mercado, L., Sitch, S., Jones, C., Gedney, N., Best, M., et al. (2011). The Joint UK
112 Land Environment Simulator (JULES), model description - Part 2: Carbon fluxes and
113 vegetation dynamics. *Geosci. Model Dev.* , 4, 701-722.

114 Clark, J., Bell, D., Chu, C., Courbaud, B., Dietze, M., Hersh, M., et al. (2010). High-
115 dimensional coexistence based on individual variation: a synthesis of evidence. *Ecol. Monogr.*
116 , 80, 569-608.

117 Collalti, A. (2011). *Sviluppo di un modello ecologico-forestale per foreste a struttura
118 complessa*. Viterbo, University of Tuscia: PhD. Thesis.

119 Collalti, A., Perugini, L., Santini, M., Chiti, T., Nolè, A., Matteucci, G., et al. (2014). A
120 process-based model to simulate growth in forests with complex structure:Evaluation and use

121 of 3D-CMCC Forest Ecosystem Model in a deciduous forest in Central Italy. *Ecological*
122 *Modelling* , 362-378.

123 Cox, P., & Jones, C. (2008). Illuminating the MOdern Dance of Climate and CO2. *Science* ,
124 321, 1642-1644.

125 Curiel Yuste, J., Janssens, I., & Cuelmans, R. (2005). Calibration and validation of an
126 empirical approach to model soil CO2 efflux in a deciduous forest. *Biogeochemistry* , 73:
127 209-230.

128 Dalmonech, D., Zaehle, S., Schurmann, G., Brovkin, V., Reick, C., & Schnur, R. (2015).
129 Separation of the Effects of Land and Climate Model Errors on Simulated Contemporary
130 Land Carbon Cycle Trends in the MPI Earth System Model version 1. *J. Climate* , 28, 272-
131 291.

132 Davidson, E., Janssens, I., & Luo, Y. (2006). On the variability of respiration in terrestrial
133 ecosystems : moving beyond Q(10). *Global Change Biology* , 12: 154-164.

134 De Pury, D., & Farquhar, G. (1997). Simple scaling of photosynthesis from leaves to canopies
135 without the errors of big-leaf models. *Plant Cell Environ.* , 20, 537-557.

136 Delpierre, N., Soudani, K., Francois, C., Kostner, B., Pontailler, J.-Y., Nikinmaa, E., et al.
137 (2009). Exceptional carbon uptake in European forests during the warm spring of 2007: a
138 data-model analysis. *Global Change Biology* , 15, 1455-1474.

139 Dickmann, D., & Kozlowski, T. (1970). Photosynthesis by rapidly expanding green strobili of
140 *Pinus resinosa*. *Life science* , 9, 549-552.

141 Dietze, M. C., Vargas, R., Richardson, A. D., Stoy, P. C., Barr, A., & Anderson, e. a. (2011).
142 Characterizing the performance of ecosystem models across time scales: A spectral analysis
143 of the North American Carbon Program site-level synthesis,. *Journal of Geophysical*
144 *Research* .

145 Dufrene, E., Davi, H., Fracois, C., le Maire, G., Le Dantec, V., & Granier, A. (2005).
146 Modelling carbon and water cycles in beech forest. Part I: Model description and uncertainty
147 analysis on modelled NEE. *Ecological Modelling* , 185: 407-436.

148 Falge, E., Baldocchi, D., Tenhunen, J., Aubinet, M., Bakwin, P., Berbigier, P., et al. (2002).
149 Seasonality of ecosystem respiration and gross primary production as derived from
150 FLUXNET measurements. *Agrocoltural and Forest Meteorology* , 113, 53-74.

151 Farquhar, G., & Sharkey, T. (1982). Stomatal conductance and photosynthesis. *Annual Review*
152 *of Plant Physiology* , 33, 317-345.

153 Farquhar, G., von Caemmerer, S., & Berry, J. (1980). A biogeochemical model of
154 photosynthetic CO₂ assimilation in leaves of C3 species. *Planta* , 149, 78-90.

155 Feikema, P., Morris, J., Beverly, C. C., Baker, T., & Lane, P. (2010). Validation of plantation
156 transpiration in south-eastern Australia estimated using the 3PG+ forest growth model. *Forest*
157 *Ecology and Management* , 260, 663-678.

158 Friedlingstein, P., Cox, P., Betts, R., Bopp, L., Von Bloh, W., Brovkin, V., et al. (2006).
159 Climate-carbon cycle feedback analysis: results from the C4MIP model intercomparison. *J.*
160 *Climate* , 19, 3337-3353.

161 Gielen, B., De Vos, B., Campioli, M., Neirynck, J., Papale, D., Verstraen, A., et al. (2013).
162 Biometric and eddy covariance-based assessment of decadal carbon sequestration of a
163 temperate Scots pine forest. *Agricultural and Forest Meteorology* , 174-175; 135-143.

164 Gough, C., Flower, C., Vogel, C., Dragoni, D., & Curtis, P. (2009). Whole-ecosystem labile
165 carbon production in a north temperate deciduous forest. *Agricultural and Forest*
166 *Meteorology* , 149, 1531-1540.

167 Granier, A., Ceschia, E., Damesin, C., Dufrene, E., Epron, D., Gross, P., et al. (2000). The
168 carbon balance of a young beech forest. *Functional Ecology* , 14, 312-325.

169 Granier, A., Reichstein, M., Brèda, N., Janssens, I., Falge, E., Ciais, P., et al. (2007).
170 Evidence for soil water control on carbon and water dynamics in European forests during the
171 extremely dry year: 2003. *Agricultural and Forest Meteorology* , 143, 123-145.

172 Griffin, K., Tissue, D., Turnbull, M., Schuster, W., & Whitehead, D. (2001). Leaf dark
173 respiration as a function of canopy position in *Nothofagus fusca* trees grown at ambient and
174 elevated CO₂ partial pressure for 5 years. *Functional Ecology* , 15, 497-505.

175 Grote, R., Korhonen, J., & Mammarella, I. (2011). Challenges for evaluating process-based
176 models of gas exchange at forest sites with firs of various species. *Forest systems* , 20(3),
177 389-406.

178 Grünwald, T., & Bernhofer, C. (2007). A decade of carbon, water and energy flux
179 measurements of an old spruce forest at the Anchor Station Tharandt. *Tellus* , 59B: 387-396.

180 Gu, L., Baldocchi, D., Verma, D., Black, T., Vesala, T., Falge, E., et al. (2002). Advantages
181 of diffuse radiation for terrestrial ecosystem productivity . *J. Geophys. Res.* , 107.

182 Guidolotti, G., Rey, A., D'Andrea, E., Matteucci, G., & De Angelis, P. (2013). Effect of
183 environmental variables and stand structure on ecosystem respiration components in a
184 Mediterranean beech forest. *Tree Physiology* , 00, 1-13.

185 He, M. J., Zhou, Y., J.M., C., He, H., Wang, S., Wang, H., et al. (2013). Development of a
186 two-leaf light use efficiency model for improving the calculation of terrestrial gross primary
187 production. *Agr. Forest Meteorol.* , 173, 28-39.

188 Hui, D., Luo, Y., & Katul, G. (2003). Partitioning interannual variability in net ecosystem
189 exchange between climatic variability and functional change. *Tree Physiology* , 23, 433-442.

190 Huntingford, C., Lowe, J., Booth, B., Jones, C., Harris, G., Gohar, L., et al. (2009).
191 Contributions of carbon cycle uncertainty to future climate projection spread. *Tellus B* , 61,
192 355-360.

193 Ibrom, A., Jarvis, P., Clement, R., Morgenstern, K., Oltchev, A., Medlyn, B., et al. (2006). A
194 comparative analysis of simulated and observed photosynthetic CO₂ uptake in two coniferous
195 canopies. *Tree Physiology* , 26, 845-864.

196 Ibrom, A., Oltchev, A., June, T., Kreilein, H., Rakkibu, G., Ross, T., et al. (2008). Variation
197 in photosynthetic light-use efficiency in a mountains tropical rain forest in Indonesia. *Tree
198 Physiol.* , 28, 499-508.

199 Janssens, I., Freibauer, A., Ciais, P., Smith, P., Nabuurs, G.-J., Folberth, G., et al. (2003).
200 Europe's Terrestrial Biosphere Absorbs 7 to 12% of European Anthropogenic CO₂ emissions.
201 *Science* , 300, 1538-1542.

202 Janssens, I., Sampson, D., Curiel Yuste, J., Carrara, A., & Ceulemans, R. (2002). The carbon
203 cost of fine root turnover in a Scots pine forest. *Forest Ecology and Management* , 168: 231-
204 240.

205 Jeong, S., Medvigy, D., Shevlankova, E., & Malyshev, S. (2013). Predicting changes in
206 temperate forest budburst using continental-scale observations and models. *Geophys. Res.
207 Lett.* , 40, 1-6.

208 Jolly, W., Dobberlin, M., Zimmerman, N., & Reichstein, M. (2005). Divergent vegetation
209 growth responses to the 2003 heat wave in the Swiss Alps. *Geophys. Res. Lett.* ,
210 doi:10.1029/2005GL023027.

211 Keenan, T., Baker, I., Barr, A., Ciais, P., Davis, K., Dietze, M., et al. (2012). Terrestrial
212 biosphere model performances for inter-annual variability of land-atmosphere CO₂ exchange.
213 *Global Change Biology* , 18(6): 1971-1987.

214 Kimball, J., Thornton, P., White, M., & Running, S. (1997). Simulating forest productivity
215 and surface-atmosphere carbon exchange in the BOREAS study region. *Tree Physiology* , 17,
216 589-599.

217 Knohl, A., Schulze, E.-D., Kolle, O., & Buchmann, N. (2003). Large carbon uptake by an
218 unmanaged 250-year-old deciduous forest in Central Germany. *Agricultural and Forest
219 Meteorology* , 118, 151-167.

220 Kobe, R. (1996). Intraspecific variation in sapling mortality and growth predicts geographic
221 variation in forest composition. *Ecol. Monogr.* , 66, 181-201.

222 Kolari, P., Pumpanen, J., Kumala, L., Ilvesniemi, H., Nikinmaa, E., Gronholm, T., et al.
223 (2006). Forest floor vegetation plays an important role in photosynthetic production of boreal
224 forests. *Forest Ecol. Manag.* , 221, 241-248.

225 Kramer, K., Leinonen, I., Bartelink, H., Berbigier, P., Borghetti, M., Bernhofer, C., et al.
226 (2002). Evaluation of six process-based forest growth models using eddy-covariance
227 measurements of CO₂ and H₂O fluxes at six forest sites in Europe. *Global Change Biology* ,
228 8, 212-230.

229 Krishnan, P., Black, T., Barr, A., Grant, N., Gaumont-Guay, D., & Nesic, Z. (2008). Factors
230 controlling the interannual variability in the carbon balance of southern boreal black spruce
231 forest. *Journal of Geophysical Research* , 113, 1-16.

232 Krishnan, P., Black, T., Jassal, R., Chen, B., & Nesic, Z. (2009). Interannual variability of the
233 carbon balance of a southern boreal black spruce forest. *Journal of Geophysical Research* ,
234 114, 1-18.

235 Landhausser, S. (2010). Aspen shoots are carbon autonomous during budbreak. *Tree* , 25- 531-
236 536.

237 Landsberg, J. (1996). *Physiological Ecology of Forest Production*. Sydney, Australia:
238 Academic Press.

239 Landsberg, J., & Waring, R. (1997). A generalised model of forest productivity using
240 simplified concepts of radiation-use efficiency, carbon balance and partitioning. *Forest*
241 *Ecology and Management* , 172, 199–214.

242 Larcher, W. (2003). *Physiological plant ecology: ecophysiology and stress physiology of*
243 *functional groups*. New York: Springer.

244 Lawrence, D., Oleson, K., Flanner, M., Thornton, P., Swenson, S., Lawrence, P., et al. (2011).
245 Parameterization Improvements and Functional and Structural Advances in Version 4 of the
246 Community Land Model. *J. Adv. Model. Earth Syst* , 3, 1-27.

247 Leuning, R., Kelliher, F., DePury, D., & Schulze, E. (1995). Leaf nitrogen, photosynthesis,
248 conductance and transpiration: Scaling from leaves to canopy . *Plant Cell Environ.* , 18, 1183-
249 1200.

250 Li, H., Sheffield, J., & Wood, E. (2010). Bias correction of monthly precipitation and
251 temperature fields from Intergovernmental Panel on Climate Change AR4 models using
252 equidistant quantile matching. *Journal of Geophysical Research* , DOI:
253 10.1029/2009JD012882.

254 Liu, Z., Wang, L., & Wang, S. (2014). Comparison of Different GPP Models in China Using
255 MODIS Image and ChinaFLUX Data. *Remote Sensing* , 6, 10215-10231.

256 Loustau, D., Bosc, A., Colin, A., Ogée, J., Davi, H., Francois, C., et al. (2005). Modelling
257 climate change effects on the potential production of French plains forests at the sub-regional
258 level. *Tree Physiology* , 25, 813-823.

259 Luyssaert, S., Abril, G., Andres, R., Bastviken, D., Bellasen, V., Bergamaschi, P., et al.
260 (2012). The European CO₂, CO, CH₄, and N₂O balance between 2001 and 2005 .
261 *Biogeosciences Discussion* , doi:10.5194/bgd-9-2005-2012.

262 Luyssaert, S., Inglima, I., Jung, M., Richardson, D., Reichstein, M., Papale, D., et al. (2007).
263 CO₂ balance of boreal, temperate, and tropical forests derived from a global database. *Global*
264 *Change Biology* , 13, 2509-2537.

265 Magnani, F., Mencuccini, M., Borghetti, M., Berbigier, P., Delzon, S., & al., e. (2007). The
266 human footprint in the carbon cycle of temperate and boreal forests. *Nature* , 447, 848-850.

267 Mahecha, M., Reichstein, M., Carvalhais, N., Lasslop, G., Lange, H., Seneviratne, S., et al.
268 (2010). Global Convergence in the Temperature Sensitivity of Respiration at Ecosystem
269 Level. *Science* , 329, 838-840.

270 Makela, A., Landsberg, J., Ek, A., Burk, T., Ter-Mikaelian, M., Agren, G., et al. (2000).
271 Process-based models for forest ecosystem management: current state of the art and
272 challenges for practical implementation. *Tree Physiology* , 20: 289,298.

273 Makela, A., Pulkkinen, M., Kolari, P., Lagergren, F., Berbigier, P., Lindroth, A., et al. (2008).
274 Developing an empirical model of stand GPP with the LUE approach: analysis of eddy
275 covariance data at five contrastinf conifer sites in Europe. *Global Change Biology* , 14, 92-
276 108.

277 Marconi, S. (2014). *Assessing NEE and Carbon Dynamics among 5 European Forest types: Development and Validation of a new Phenology and Soil Carbon routines within the process oriented 3D-CMCC-Forest Ecosystem Model*. Viterbo: Master thesis, University of Tuscia.

280 Marks, D., Dozier, J., & Davies, R. (1992). Climate and energy exchange at the snow surface
281 in the alpine region of the Sierra Nevada. I. Meteorology measurments and monitoring. *Water
282 Resouces Research* , 4, 719-739.

283 Medlyn, B., Dreyer, E., Ellsworth, D., Forstreuter, M., Harley, P., Kirschbaum, M., et al.
284 (2003). Temperature response of parameters of a biogeochemically based model of
285 photosynthesis. II. A review of experimental data. *Plant, Cell & Environment* , 25, 1167-
286 1179.

287 Mercado, L., Bellouin, N., Sitch, S., Boucher, O., Huntingford, C., Wild, M., et al. (2009).
288 Impact of changes in diffuse radiation on the global land carbon sink. *Nature* , 458, 1014-
289 1017.

290 Migliavacca, M., Reichstein, M., Richardson, A., Mahecha, D., Cremonese, E., DelPierre, N.,
291 et al. (2015). Influence of physiological phenology on the seasonal patterns of ecosystem
292 respiration in deciduous forests. *Global Change Biology* , 21, 363-376.

293 Misson, L., Baldocchi, D., Black, T., Blanken, P., Brunet, Y., Curiel Yuste, J., et al. (2007).
294 Partitioning forest carbon fluxes with overstory and understory eddy-covariance
295 measurements: A synthesis based on FLUXNET data. *Agricultural and Forest Meteorology* ,
296 144, 14-31.

297 Mollicone, D., Matteucci, G., Koble, R., Masci, A., Chiesi, M., & Smits, P. (2003). A Model-
298 Based Approach for the Estimation of Carbon Sinks in European Forests. In R. Valentini,
299 *Fluxes in Carbon, Water and Energy of European Forests* (pp. 164, 179-205). Heidelberg:
300 Springer-Verlag .

301 Montagnani, L., Manca, G., Canepa, E., Georgieva, E., Acosta, M., Feigenwinter, C., et al.
302 (2009). A new mass conservation approach to the study of CO₂ advection in an alpine forest.
303 *Journal of Geophysical Research* , 114: D07306.

304 Monteith, J. (1977). *Climate and the efficiency of crop production in Britain*. London: Phil.
305 Trans. Roy. Soc.

306 Monteith, J. (1965). Evaporation and environment. In J. Monteith, *Symposium, Society of*
307 *Experimental Botany* (pp. 19, 205-234). Cambridge: Cambridge University Press.

308 Morales, P., Sykes, M., Prentice, I., Smith, P., Smith, B., Bugmann, H., et al. (2005).
309 Comparing and evaluating process-based ecosystem model predictions of carbon and water
310 fluxes in major European forest biomes. *Global Change Biology* , 11, 2211-2233.

311 Nabuurs, G., Schelhaas, M., Mohren, G., & Field, C. (2003). Temporal evolution of the
312 European forest sector carbon sink from 1950 to 1999. *Global Change Biology* , 9, 152-160.

313 Naudts, K., Ryder, J., McGrath, M., Otto, J., Chen, Y., Valade, A., et al. (2014). A vertically
314 discretised canopy description for ORCHIDEE (SVN r2290) and the modifications to the
315 energy, water and carbon fluxes. *Geosci. Model Dev. Discuss.* , 7, 8565-8647.

316 Nolè, A., Collalti, A., Magnani, F., Duce, P., Ferrara, A., Mancino, G., et al. (2013).
317 Assessing temporal variation of primary and ecosystem production in two Mediterranean
318 forests using a modified 3-PG model. *Annals of Forest Science* , DOI 10.1007/s13595-013-
319 0315-7.

320 Ogren, E. (2000). Maintenance respiration correlates with sugar but not nitrogen
321 concentration in dormant plants. *Physiologia Plantarum* , 108:295-299.

322 Oltchev, A., Cermak, J., Nadezhina, N., Tatarinov, F., Tishenko, A., Ibrom, A., et al. (2002).
323 Transpiration of a mixed forest stand: field measurements and simulation using SVAT
324 models. *Boreal Environment Research* , 7, 389-397.

325 Papale, D., Reichstein, M., Aubinet, M., Canfora, E., Bernhofer, C., Kutsch, W., et al. (2006).
326 Towards a standardized processing of Net Ecosystem Exchange measured with eddy
327 covariance technique: algorithms and uncertainty estimation. *Biogeosciences* , 3, 571-583.

328 Peters, W., Jacobson, A., Sweeney, C., & al., e. (2007). An atmospheric perspective on North
329 American carbon dioxide exchange: carbontracker. *Proceedings of the National Academy of
330 Sciences of the United States of America* , 104, 18925-18930.

331 Piao, S., Friedlingstein, P., Ciais, P., Zhou, L., & Chen, A. (2006). Effects of climate and CO2
332 changes on the greening of the Northern Hemisphere over the past two decades. *Geophys.
333 Res. Lett.* , 33, L23402, doi:10.1029/2006GLO28205.

334 Piao, S., Sitch, S., Ciais, P., Friendlingstein, P., Peylin, P., Wang, X., et al. (2013). Evaluation
335 of terrestrial carbon cycle models for their response to climate variability and to CO2 trends.
336 *Global Change Biology* , 19, 2117-2132.

337 Pietsch, S., Hasenauer, H., & Thornton, P. (2005). BGC-model parameters for tree species
338 growing in central European forests. *Forest Ecology and Management* , 211, 264-295.

339 Pilegaard, K., Ibrom, A., Courtney, M., Hummelshoj, P., & Jensen, N. (2011). Increasing net
340 CO2 uptake by a Danish beech forest during the period from 1996 to 2009. *Agrocoltural and
341 Forest Meteorology* , 151: 934-946.

342 Poulter, B., Heyder, U., & Cramer, W. (2009). Modelling the Sensitivity of the Seasonal
343 Cycle of GPP to Dynamic LAI and Sil Depths in Tropical Rainforest. *Ecosystems* , 12, 517-
344 533.

345 Poulter, B., MacBean, N., Hartley, A., Khlystova, I., Arino, O., Betts, R., et al. (2015). Plant
346 functional type classification for Eart System Models: results from the European Space
347 Agency's Land Cover Climate Change Initiative. *Geosci. Model Dev. Discuss.* , 8, 429-462.

348 Prentice, I., Liang, B., B.E., M., & Wang, Y.-P. (2014). Reliable, robust and realistic: the
349 three R's of next-generation land surface modelling. *Atmos. Chem. Phys. Discuss.* , 14, 24811-
350 24861.

351 Propastin, P., Ibrom, A., Knohl, A., & Erasmi, S. (2012). Effects of canopy photosynthesis
352 saturation on the estimation of gross primary productivity from modis datain a tropical forest.
353 *Remote Sens. Environ.* , 121, 252-260.

354 Reichstein, M., Falge, E., Baldocchi, D., Papale, D., Valentini, R., Aubinet, M., et al. (2005).
355 On the separation of net ecosystem exchange into assimilation and ecosystem respiration:
356 review and improved algorithm. *Global Change Biology* , 11, 1424-1439.

357 Reichstein, M., Tenhunen, J., Roupsard, O., Ourcival, J.-M., Rambal, S., Dore, S., et al.
358 (2002). Ecosystem respiration in two Mediterranean evergreen Holm Oak forests: drought
359 effects and decomposition dynamics. *Functional Ecology* , 16, 27-39.

360 Richardson, A., Anderson, R., Altafarain, M., Barr, A., Bohrer, G., Chen, G., et al. (2012a).
361 Terrestrial biosphere models need better representation of vegetation phenology: results from
362 the North American Carbon Program Site Synthesis. *Global Change Biology* , 18, 566-584.

363 Richardson, A., Aubinet, M., Barr, A., Hollinger, D., Ibrom, A., Lasslop, G., et al. (2012b).
364 Uncertainty quantification. In M. Aubinet, T. Vesala, & D. Papale, *Eddy Covariance*.
365 Heidelberg London New York: Springer Dordbrecht.

366 Richardson, A., Black, T., Ciais, P., Delbart, N., Friedl, M., Gobron, N., et al. (2010).
367 Influence of spring and autumn phenological transitions on forest ecosystem productivity.
368 *Phyl. Trans. R. Soc. B.* , 365, 3227-3246.

369 Richardson, A., Hollinger, D., Aber, J., Ollinger, S., & Braswell, B. (2007). Environmental
370 variation is directly responsible for short- but not long-term variation in forest-atmosphere
371 carbon exchange. *Global Change Biology* , 13, 788-803.

372 Rotzer, T., Grote, R., & H., P. (2004). The timing of bud burst and its effect on tree growth.
373 *Internation Journal of Biometeorology* , 48, 109-118.

374 Ruimy, A., Jarvis, P., Baldocchi, D., & Sugier, B. (1995). CO₂ fluxes over plant canopies and
375 solar radiation: A review. *Adv. Ecol. Res.* , 26, 1-51.

376 Running, S., & Coughlan, J. (1988). A general model of forest ecosystem processes for
377 regional applications I. Hydrologic balance, Canopy Gas Exchange and Primary Production
378 Processes. *Ecological Modelling* , 42:125-154.

379 Ryan, M. (1991). Effects of climate change on plant respiration. *Ecological Applications* ,
380 1:157-167.

381 Sabatè, S., Gracia, C., & Sàncchez, A. (2002). Likely effects of climate change on growth of
382 Quercus ilex, Pinus halepensis, Pinus pinaster, Pinus sylvestris and Fagus sylvatica forests in
383 the Mediterranean region. *Forest Ecology and Management* , 162, 23-37.

384 Santini, M., Collalti, A., & Valentini, R. (2014). Climate change impacts on vegetation and
385 water cycle in the Euro-Mediterranean region, studied by a likelihood approach. *Reg.*
386 *Environ. Change* , DOI 10.1007/s10113-013-0582-8.

387 Scartazza, A., Moscatello, S., Matteucci, G., Battistelli, A., & Brugnoli, E. (2013). Seasonal
388 and inter-annual dynamics of growth, non-structural carbohydrates and C stable isotopes in
389 Mediterranean beech forest. *Tree Physiology* , 730-742.

390 Seidl, R., Rammer, W., Scheller, R., & Spies, T. (2012). An individual-based process model
391 to simulate landscape-scale forest ecosystem dynamics. *Ecological Modelling* , 231, 87-100.

392 Sellers, P., Dickinson, R., Randall, D., & al., e. (1997). Modelling the exchanges of energy,
393 water, and carbon between continents abd the atmosphere. *Science* , 275, 502-509.

394 Shinozaki, K., Yoda, K., Hozumi, K., & Kira, T. (1964a). A quantitative analysis of plant
395 form-the pipe model theory. I Basic analyses. *Japanese Journal of Ecology* , 4, 97-105.

396 Shinozaki, K., Yoda, K., Hozumi, K., & Kira, T. (1964b). A quantitative analysis of plant
397 form-the pipe model theory. II. Further evidence of the theory and its application in forest
398 ecology. *Japanese Journal of Ecology* , 14, 133-139.

399 Slevin, D., Tett, S., & Williams, M. (2015). Multi-site evaluation of the JULES land surface
400 model using global and local data. *Geosci. Model Dev.* , 8, 295-316.

401 Suni, T., Berninger, F., Vesala, T., Markkanen, T., Hari, P., Makela, A., et al. (2003). Air
402 temperature triggers the recovery of evergreen boreal forest photosynthesis in spring. *Global*
403 *Change Biology* , 9, 1410-1426.

404 Suni, T., Berninger, F., Vesala, T., Markkanen, T., Hari, P., Makela, A., et al. (2003). Air
405 temperature triggers the recovery of evergreen boreal forest photosynthesis in spring. *Global*
406 *Change Biology* , 9, 1410-1426.

407 Sykes, M., Prentice, I., Smith, B., Cramer, W., & Venevsky, S. (2001). An introduction to the
408 European terrestrial ecosystem modelling activity. *Global Ecol. Biogeogr.* , 10, 581-594.

409 Taylor, K. (2001). Summarizing multiple aspects of model performance in a single diagram.
410 *Journal of Geophysical Research* , 106, 7183-7192.

411 Taylor, K., Stouffer, R., & Meehl, G. (2012). An overview of CMIP5 and the experiment
412 design. *Bull. Am. Meteorol. Soc.* , 90, 485-498.

413 Thornton, P. E. (2010). *Biome BGC version 4.2: Theoretical Framework of Biome-BGC*.

414 Thornton, P., & Zimmermann, N. (2007). An Improved Canopy Integration Scheme for a
415 Land Surface Model with Prognostic Canopy Structure. *Journal of Climate* , 20, 3902-3923.

416 Turner, D. U., Bremer, D., Wofsy, S., Meyers, T., Gower, S., & Gregory, M. (2003). A cross-
417 biome comparison of daily light use efficiency for gross primary production. *Global Change
418 Biol.* , 9, 383-395.

419 UNECE, & FAO. (2011). *State of Europe's Forest*. Status and Trends in Suistainable Forest
420 Management in Europe.

421 Verbeeck, H., Steppe, K., Nadezhina, N., Op De Beeck, M., Meiresonne, L., Lemeur, R., et
422 al. (2007). Model analysis of the effects of atmospheric drivers on storage water use in Scots
423 pine. *Biogeosciences* , 4, 657-671.

424 Vetter, M., Churkina, G., Jung, M., Reichstein, M., Zaehle, S., Bondeau, A., et al. (2008).
425 Analyzing the causes and spatial pattern of the European 2003 carbon flux anomaly using
426 seven models. *Biogeosciences* , 5, 561-583.

427 Vitale, M., Scimone, M., Feoli, E., & Manes, F. (2003). Modelling leaf gas exchanges to
428 predict functional trends in Mediterranean Quercus ilex forest under climatic changes in
429 temperature. *Ecological Modelling* , 166, 123-134.

430 Wang, F., Chen, J., Gonsamo, A., Zhou, B., Cao, F., & Yi, Q. (2014a). A two-leaf rectangular
431 hyperbolic model for estimating GPP across vegetation types and climate conditions. *J.
432 Geophys. Res. Biogeosci.* , 119, doi: 10.1002/2013JG002596.

433 Wang, H., Prentice, I., & Davis, T. (2014b). Biophysical constraints on gross primary
434 production by the terrestrial biosphere. *Biogeosciences* , 11, 5987-6001.

435 Waring, R., & Landsberg, J. (1998). Net primary production of forests: a constant fraction of
436 gross primary production? *Tree Physiology* , 18, 129-134.

437 Waring, R., & McDowell, N. (2002). Use of a physiological process model with forestry yield
438 tables to set limits on annual carbon balances. *Tree Physioloogy* , 22, 179-188.

439 Warren, J., Potzelsberger, E., Wullschleger, S., Thornton, P., Hasenauer, H., & Norby, R.
440 (2011). Ecohydrologic impact of reduced stomatal conductance in forests exposed to elevated
441 CO₂. *Ecohydrology* , 4, 196-210.

442 White, M., Thornton, P., & Running, S. (2000). Parameterization and sensitivity analysis of
443 the BIOME-BGC terrestrial ecosystem model: net primary production controls. *Earth*
444 *interactions* , 4 (3), 1.

445 Willmott, C., & Matsuura, K. (2005). Advantages of the mean absolute error error (MAE)
446 over the root mean square error (RMSE) in assessing average model performance. *CLIMATE*
447 *RESEARCH* , 30, 79-82.

448 Wißkirchen, K., Tum, M., Günther, K., Niklaus, B., Eisfelder, C., & Knorr, W. (2013).
449 Quantifying the carbon uptake by vegetation for Europe on a 1km² resolution using a remote
450 sensing driven vegetation model. *Geoscientific Model Development* , 6, 1623-1640.

451 Wramneby, A., Smith, B., Zaehle, S., & Sykes, M. (2008). Parameter uncertainties in the
452 modelling of vegetation dynamics-Effects on tree community structure and ecosystem
453 functioning in European forest biomes. *Ecological Modelling* , 216, 277-290.

454 Wu, J., Jansson, P., van der Linden, L., Pilegaard, K., Beier, C., & Ibrom, A. (2013).
455 Modelling the decadal trend of ecosystem carbon fluxes demonstrates the important role of
456 functional changes in a temperate deciduous forest. *Ecological Modelling* , 260, 50-61.

457 Wu, X., Ju, W., Zhou, Y., He, M., Law, B., Black, T., et al. (2015). Performance of Linear
458 and Nonlinear Two-leaf Light Use Efficiency Models at Different Temporal Scales. *Remote*
459 *sensing* , xxxx.

460 Yin, Z., Dekker, S., van den Hurk, B., & Dijkstra, H. (2014). Effects of vegetation structure
461 on biomass accumulation in a Balanced Optimally Structure Vegetation Model (BOSVM
462 v1.0). *Geosci. Model Dev.* , 7, 821-845.

463 Yuan, W., Liu, S., Zhou, G., Zhou, G., Tieszen, L., Baldocchi, D., et al. (2007). Deriving a
464 light use efficiency model from eddy covariance flux data for predicting daily gross primary
465 production across biomes. *Agricultural and Forest Meteorology* , 143, 189-207.

466 Zeng, D., Hunt, E., & Running, S. (1993). A Daily Soil Temperature Model Based on Air
467 Temperature and Precipitation for Continental Applications. *Climate Research* , 2, 183-191.

468 Zhang, T., Lichstein, J., & R.A., B. (2014). Spatial and temporal heterogeneity in the
469 dynamics of eastern U.S. forests: Implications for developing broad-scale forest dynamics
470 models. *Ecological Modelling* , 279, 89-99.

471 Zhao, Y., Ciais, P., Peylin, P., Viovy, N., Longdoz, B., Bonnefond, J., et al. (2012). How
472 errors on meteorological variables impact simulated ecosystem fluxes: a case study for six
473 French sites. *Biogeosciences* , 9, 2537-2664.

474 Zscheischler, J., Michalak, A., Schwalm, C., Mahecha, M., Huntzinger, D., Reichstein, M., et
475 al. (2014). Impact of large-scale climate extremes on biospheric carbon fluxes: An
476 Intercomparison based on MsTMIP data. *Global Biogeochemical Cycles* , 28, 585-600.

477

478